# Regimes of Conformational Transitions of a Diblock Polyampholyte

**Zuowei Wang and Michael Rubinstein***

*Department of Chemistry, University of North Carolina, Chapel Hill, North Carolina 27599-3290*

*Received April 3, 2006; Revised Manuscript Received June 12, 2006*

ABSTRACT: The conformational properties of symmetric flexible diblock polyampholytes are investigated by scaling theory and molecular dynamics simulations. The electrostatically driven coil−globule transition of a symmetric diblock polyampholyte is found to consist of three regimes identified with increasing electrostatic interaction strength. In the first (folding) regime the electrostatic attraction causes the chain to fold through the overlap of the two blocks, while each block is slightly stretched by self-repulsion. The second (weak association or scrambled egg) regime is the classical collapse of the chain into a globule dominated by the fluctuation-induced attractions between oppositely charged sections of the chain. The structure of the formed globule can be represented as a dense packing of the charged chain sections (electrostatic attraction blobs). The third (strong association or ion binding) regime starts with direct binding of oppositely charged monomers (dipole formation), followed by a cascade of multipole formation (quadrupole, hexapole, octupole, etc.), leading to multiplets analogous to those found in ionomers. The existence of the multiplet cascade has also been confirmed in the simulations of solutions of short polymers with only one single charge (either positive or negative) in the middle of each chain. We use scaling theory to estimate the average chain size and the electrostatic correlation length as functions of the chain length, strength of electrostatic interactions, charge fraction, and solvent quality. The theoretically predicted scaling laws of these conformational properties are in very good agreement with our simulation results.

## 1. Introduction

If macromolecules with ionizable groups dissolve in polar solvents, these groups dissociate, leaving charges on polymers and releasing counterions into solution. Charged polymers can be classified into polyelectrolytes with a single sign of charged monomers and polyampholytes with both positive and negative charges on the same chain.[1−5] These macromolecules are often water-soluble and have numerous industrial applications. Synthetic charged polymers can also be regarded as model systems for electrostatic interactions in biomolecules, such as DNA, RNA, and proteins.

The solutions containing mixtures of oppositely charged polymers exhibit rich aggregation and phase separation behavior, depending on their stoichiometry, i.e., the charge densities, the relative concentrations, and chain lengths.[4,6−16] If a mixture of oppositely charged polyelectrolytes is symmetric in charge, i.e., the polycations and polyanions carry the same absolute amount of charges and have the same concentrations, it phase separates into a dense sediment and a very dilute supernatant. On the other hand, soluble aggregates carrying a net charge, called polyelectrolyte complexes, can be formed in the asymmetric mixtures.[6−10,13−16]

Mixtures of random polyampholytes with excess charges of both positive and negative signs also have a strong tendency to associate into neutral complexes and precipitate.[11,12] Solutions of polyampholytes with zero net charge on the chains phase separate at very low concentrations. The supernatant is dominated by a very dilute mixture of charge-compensated unimers and clusters with zero net charge that form spherical globules. In solutions with excess of either positively or negatively charged chains, the free counterions escape into the supernatant together with the most strongly charged chains.[11] These dissolved polyampholyte chains in the dilute phase form necklace-like intramolecular structures.[4,17−20]

A change of polymer architecture from random to block polyampholytes leads to a significant change in solution properties.[21−25] The block polyampholytes are composed of charged blocks (polyelectrolytes) of opposite signs chemically linked by their ends. The localization of the same-sign charges within one block increases the electrostatic attraction between oppositely charged sections. It results in a more extensive precipitation at the isoelectric point where the net charge of the chains vanishes. At pH values above or below the isoelectric point, block polyampholytes can associate into soluble micelles. The micelle formation has been experimentally observed in solutions of diblock polyampholytes.[21−23] One principal advantage of these block polyampholytes is that their association and stabilization behavior can be easily regulated by adjusting the pH values of the solutions. This may lead to many potential applications and thus stimulates increasing experimental and theoretical interests in these materials.

The scaling theory for diblock polyampholytes has been developed by Castelnovo and Joanny for solutions with high ionic strength[24] and by Shusharina et al. for salt-free solutions.[25] In ref 25 it is shown that a charge-symmetric diblock polyampholyte chain with equally charged positive and negative blocks collapses into a globule, while a charge-asymmetric block polyampholyte has a tadpole shape with a globular head and a polyelectrolyte tail. If the electrostatic repulsion energy between tadpoles is weaker than the surface energy gain due to coalescence of their globular heads, tadpoles associate into micelles. The association of block polyampholytes is driven by the charge density fluctuation-induced attractive interactions between oppositely charged blocks.[24,25] This so-called "scrambled-egg" model of electrostatic attraction has also been used to describe the complexation of oppositely charged polyelectrolytes.[26,27] Shusharina et al.[25] predicted that the chains in a micelle should partition (disproportionate) between the core and the corona. These diblock polyampholytes are divided into two populations, with one group completely confined inside the core while another group places higher charged blocks completely

* Corresponding author. E-mail: mr@unc.edu.

10.1021/ma0607517 CCC: $33.50 
Published on Web 07/21/2006

in the corona. The disproportionation of chain conformations in a micelle[25] lowers the total free energy and thus results not only in larger aggregation numbers, as compared to the case where all chains are in a similar conformation with the same fraction of longer blocks forming the corona,[24] but also in the enhanced stability of the homogeneous solution. Micelles with disproportionated chains remain stable even if the net charge of each block polyampholyte is as small as one elementary charge per chain.

Computer simulations have also been used to investigate diblock polyampholyte systems. Imbert et al.[28] and Baumketner et al.[29] have performed simulations to study the conformational properties of a single diblock polyampholyte with symmetric blocks. These works considered chains of rather short length and were restricted to the high charge fraction limit ($f = 1$) where all monomers along the chain are charged. The observed conformational transition was interpreted using the concept of pairing of consecutive oppositely charged monomers,[28] similar to the so-called "zipper" model that was applied to describe the complexation of oppositely charged polyelectrolytes.[26,27] The term "zipper" refers to the formation of strong bonds between complementary sequences of oppositely charged groups along the chains. A related problem studied by computer simulations is the aggregation of two oppositely charged polyelectrolytes.[8,14] The two oppositely charged chains remain separated at small values of interaction strength but aggregate into compact complexes analogous to the collapsed diblock polyampholyte globule at large interaction strengths.[14] Grand canonical Monte Carlo simulations have been performed to study the phase diagram of diblock polyampholyte solutions.[30] The simulation results show that as the chain length increases, the critical temperature increases while the critical volume fraction decreases. The critical temperature of diblock polyampholytes is much higher and has a stronger chain length dependence than the critical temperature of random polyampholytes. Spherical brushes composed of diblock polyampholytes end-grafted onto spherical particles have also been investigated by Monte Carlo simulations.[31] The structure of the grafted polyampholyte layer changes with the variation of the charge ratio between the two blocks from the extended polyelectrolyte brush to the collapsed polyelectrolyte complex surrounding the particle and to the inverted polyelectrolyte brush.

The single chain behavior of polyampholytes with other charge arrangements, such as random, alternating, or multiblocks, has also been extensively studied by computer simulations.[4,18−20,32−34] The case of alternating charges is well understood in terms of the collapse due to effectively short-ranged interactions similar to the coil−globule transition of uncharged polymers.[32,35] For polyampholytes with random sequence of oppositely charged monomers, the overall excess charge $Q$ on the molecules is the main factor determining the chain size.[17,18,36] Chains consisting of $N$ monomers with charge fraction $f$ and net charge $Q$ less than $(fN)^{1/2}$ behave similar to a polyampholyte with zero net charge ($Q = 0$) and collapse into spherical globules as predicted by Higgs and Joanny.[37] Stronger charged chains with $|Q| > (fN)^{1/2}$ adopt elongated conformations of pearl-necklace-like sequences of smaller globules connected by thin strings.[4,19,38] The ensemble-average chain size of randomly charged polyampholytes is dominated by these extended chains and grows as $N^{1/2}$.[19]

The aim of our paper is to present a systematic investigation on the conformational properties of a single diblock polyampholyte in order to understand the underlying physical mechanism of its coil-to-globule transition. We have performed extensive molecular dynamics (MD) simulations in a wide range of parameters such as chain length, interaction strength, and charge fraction. The simulation results are rationalized using scaling theory calculations. The rest of the paper is organized as follows: In section 2 we describe the model of diblock polyampholytes and the details of our molecular dynamics simulations. The simulation results are presented and compared with scaling theory calculations in section 3, while the diagram of conformational states of diblock polyampholytes is discussed in detail in section 4.

## 2. Model and Methodology

Diblock polyampholytes are simulated using the standard bead−spring chain model.[39−41] Each $N$-mer consists of two oppositely charged blocks. In the present paper we focus on the symmetric case with the same number of monomers ($N/2$) and the same charge fraction $f$ in each block. Since the net charge of each chain is zero, no additional counterions are needed to maintain the electroneutrality of the system. The charged and neutral monomers are arranged into a regular sequence along each block. This means that neutral spacers between two neighboring charges all consist of $1/f - 1$ uncharged monomers.

All monomers interact via a truncated-shifted Lennard-Jones (LJ) potential

$$U_{\mathrm{LJ}}(r) = \begin{cases} 4\epsilon_{\mathrm{LJ}}\left[\left(\frac{\sigma}{r}\right)^{12} - \left(\frac{\sigma}{r}\right)^{6} - \left(\frac{\sigma}{R_c}\right)^{12} + \left(\frac{\sigma}{R_c}\right)^{6}\right]; & r < R_c \\ 0; & r > R_c \end{cases} \quad (1)$$

where $r$ is the distance between the centers of two monomers and $R_c$ is the cutoff radius. The parameter $\epsilon_{\mathrm{LJ}}$ controls the strength of the short-range interactions, and the LJ diameter $\sigma$ is used to set the length scale. We present the results for both good (athermal) and Θ solvent conditions. For the good solvent condition, the cutoff $R_c$ is taken to be $2^{1/6}\sigma$ (at the minimum of the LJ potential), thus presenting a purely repulsive potential $U_{\mathrm{LJ}}$. The interaction parameter of this potential is chosen to be $\epsilon_{\mathrm{LJ}} = 1.0k_BT$, where $k_B$ is the Boltzmann constant and $T$ is the absolute temperature. For the Θ solvent, a larger cutoff $R_c = 2.5\sigma$ is utilized in order to include the attractive interaction between the monomers, and a value of $\epsilon_{\mathrm{LJ}} = 0.34k_BT$ is used for the LJ parameter, following the work of Micka, Holm, and Kremer.[40]

The connectivity of the bonded monomers is maintained by the finite extensible nonlinear elastic (FENE) potential

$$U_{\mathrm{FENE}}(r) = -\frac{1}{2}k_{\mathrm{FENE}}R_0^{\,2}\ln\left(1 - \frac{r^2}{R_0^{\,2}}\right) \quad (2)$$

where the spring constant $k_{\mathrm{FENE}} = 7k_BT/\sigma^2$ and the maximum bond length $R_0 = 2\sigma$ at which the elastic energy of the bond becomes infinite.[39,40] Solvent molecules are not included explicitly in our simulations. The solvent is modeled as a continuous dielectric medium with dielectric constant $\epsilon$ and no added salt. The charged monomers are thus interacting with each other via the unscreened Coulomb potential

$$U_{\mathrm{Coul}}(r_{ij}) = k_BT\frac{l_Bq_iq_j}{r_{ij}} \quad (3)$$

where $q_i$ is the charge valence of the $i$th particle, equal to $+1$ ($-1$) for the monovalent positive (negative) charges and 0 for the neutral monomers, and $r_{ij}$ is the distance between the centers

of *i* and *j* particles. The strength of the electrostatic interaction is represented by the Bjerrum length $l_B$ which is defined as the distance at which the electrostatic interaction energy between two elementary charges is equal to the thermal energy:

$$l_B = e^2/(\epsilon k_B T) \tag{4}$$

where *e* is the elementary charge. For the simulations of a single diblock polyampholyte with zero net charge and no counterions, the periodic boundary conditions are not necessary and the Coulomb interactions are summed over all the charged monomers directly. In section 3.3, a solution of short polymers each carrying a single charge is simulated using periodic boundary conditions. In that case the Coulomb interactions are calculated using the particle−particle−particle mesh (P3M) algorithm[42] with the optimal splitting parameters determined by the error formulas derived by Deserno and Holm.[43,44]

A velocity Verlet algorithm is utilized to integrate the equations of motion of the particles. The system is coupled to the Langevin thermostat by the standard equation[39−41]

$$m\frac{d^2\mathbf{r}_i}{dt^2} = -\nabla U(\mathbf{r}_i) - \zeta\frac{d\mathbf{r}_i}{dt} + \Gamma_i(t) \tag{5}$$

where $\mathbf{r}_i$ is the coordinate of the *i*th particle, *m* is the particle mass, and $\zeta$ is the friction coefficient equal to $\zeta = 1.0(mk_BT)^{1/2}/\sigma$. The stochastic force $\Gamma_i$ is given by a $\delta$-correlated Gaussian noise source. The time step $\Delta t$ is set to be $0.0125\tau$ in most of our simulations, where $\tau = (m\sigma^2/k_BT)^{1/2}$ is the LJ time unit. For simulations of the systems with very strong electrostatic interactions (e.g., for diblock chains with charge fraction $f = 1$ at $l_B > 8\sigma$, for chains with $f = 1/2$ at $l_B > 32\sigma$, and for chains with $f \le 1/4$ at $l_B \ge 64\sigma$, etc.), the time step is reduced to a smaller value of $\Delta t = 0.003\tau$. In this case, the total simulation time of each run ($2.4 \times 10^5\tau$) is still many times of the correlation time of the chain size as defined below.

The initial conformations of polymer chains are chosen to be self-avoiding walks with no overlap between monomers. These polymers are first relaxed as uncharged chains without Coulomb interactions for at least 10 times of the measured relaxation time of the chain size in order to get the equilibrium neutral chain conformations. Then monovalent charges are assigned to a set of monomers of each chain in a regular way so that every $1/f$ monomer of one block (one-half of the chain) is positively charged and every $1/f$ monomer of the other block is negatively charged. The generated charged chains are used as the initial configurations of the diblock polyampholytes. Each diblock polyampholyte is equilibrated for a period of $3 \times 10^6-2 \times 10^7$ MD time steps, and the physical properties of the chain are obtained by averaging over the production run of $2 \times 10^7-6 \times 10^7$ time steps after the equilibration. The simulation time for the equilibration and production periods are determined to be 10−100 times longer than the correlation time $\tau_{correl}$ of the square radius of gyration $R_g^2$, which is calculated from the exponential fit $[\exp(-t/\tau_{correl})]$ of the time correlation function

$$C_{R_g^2}(t) = \frac{\langle R_g^2(t)R_g^2(0)\rangle - \langle R_g^2\rangle^2}{\langle R_g^4\rangle - \langle R_g^2\rangle^2} \tag{6}$$

for each system. For example, $\tau_{correl}$ is found to be about $592\tau$ for uncharged chain with degree of polymerization $N = 128$ and about $2669\tau$ for uncharged chain of $N = 256$ monomers. This correlation time is shorter for the charged diblock chains at nonzero Bjerrum length, e.g., for the highly charged diblock polyampholytes ($f = 1$) with $N = 128$ and $N = 256$ monomers at $l_B = \sigma$, $\tau_{correl} \approx 240\tau$, and $314\tau$, respectively.

To confirm that the final results are independent of the initial configurations, several different initial configurations are generated and simulated for each given set of parameters *N*, *f*, and $l_B$. Various physical quantities, including the mean-square radius of gyration, the mean-square end-to-end distance, and the average total potential energy, are calculated for each individual run. Runs with different initial conditions lead to very close numerical results within the estimated error[45] of 1−2%. The small estimated errors indicate that we have achieved the equilibrium states of the chains and the simulation results are obtained from long enough runs. The only exceptions are the cases of very strong electrostatic interaction strength (e.g., $l_B \ge 50\sigma$ for diblock chains with charge fraction $f = 1/16$) with strong ion binding between oppositely charged monomers. Chains with these very strong ionic bonds are expected to be trapped in metastable states, and the results show some dependence on the initial configurations. In this case a much larger averaging over many initial configurations is needed.

### 3. Conformational Regimes

We have investigated diblock polyampholytes consisting of $N = 32$, 64, 128, 256, and 512 monomers. The charge fraction is taken to be $f = 1$, 1/2, 1/4, 1/8, 1/16, and 1/32. The simulations are first performed in the case of Bjerrum length $l_B = 0$ corresponding to the chains with no electrostatic interactions. Then the Bjerrum length is increased from $l_B = \sigma/4096$ to $l_B = 128\sigma$ in steps of factor of 2. In the region with strong ion binding between oppositely charged monomers, we have performed a denser sampling of electrostatic interactions.

The value of Bjerrum length, $l_B$, could be experimentally controlled by using solvents with different dielectric constants and changing the temperature above the freezing point of the solvents. For example, the Bjerrum length in water (dielectric constant $\epsilon = 80$) is about 7 Å at room temperature. Assuming that the monomer size of the polymer chains is about 3.5 Å, $l_B$ is equal to $2\sigma$ in water at room temperature. It is about $160\sigma$ in air and about $80\sigma$ in nonpolar solvents (toluene, benzene, chlorobenzene, etc.). There are also solvents more polar than water (such as formamide with $\epsilon = 109$ and *N*-methylformamide with $\epsilon = 182$ at $T = 298$ K) which lead to values of $l_B$ smaller than $2\sigma$. Therefore, a wide range of over 2 decades of $l_B$ values is accessible and has been experimentally investigated.[46−48] An even wider range of electrostatic interactions can be sampled numerically in order to understand different asymptotic limits.

Figure 1 presents the simulation results of the root-mean-square radius of gyration $R_g$, which is defined as

$$R_g = \left\langle \frac{1}{2N^2}\sum_{i,j=1}^{N}(\mathbf{r}_i - \mathbf{r}_j)^2 \right\rangle^{1/2} \tag{7}$$

of the diblock polyampholyte chain (solid circles) with $N = 256$ monomers and charge fraction $f = 1/4$ in a good solvent condition as a function of the Bjerrum length $l_B$. Since the two blocks of the chain are symmetric in both length and charge fraction, their average sizes are expected to be exactly the same at all values of $l_B$. This is confirmed in our simulations, and the root-mean-square radii of gyration $R_{g,blk}$ of the two individual blocks are presented by open squares in Figure 1.

The decrease of the polymer size, $R_g$, with increasing strength of electrostatic interactions, $l_B$, clearly reflects a conformational transition of the diblock polyampholyte chain from a swollen

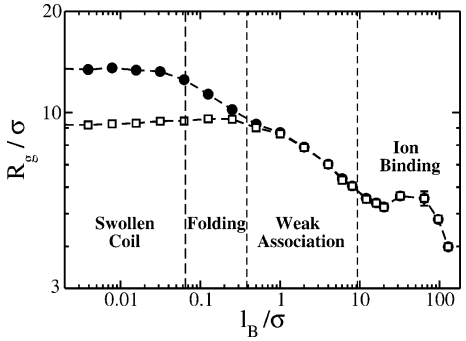


**Figure 1.** Root-mean-square radii of gyration $R_g$ of the whole chain (solid circles) and of individual blocks (open squares) as a function of the Bjerrum length $l_B$ for the diblock polyampholyte with $N = 256$ monomers and fraction of charged monomers $f = 1/4$ in a good solvent. The different regimes in the coil−globule transition are separated by the vertical dashed lines.

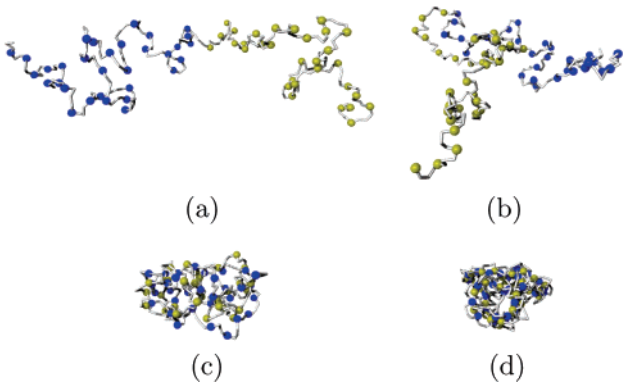


**Figure 2.** Snapshots of the diblock polyampholyte with $N = 256$ monomers and charge fraction $f = 1/4$ in a good solvent at different values of Bjerrum length: (a) $l_B = 0$ (swollen coil); (b) $l_B = \sigma/8$ (folding regime); (c) $l_B = 6\sigma$ (weak association regime); (d) $l_B = 32\sigma$ (ion binding regime). Oppositely charged monomers are presented as spheres with different colors.

coil to a compact globule. This coil−globule transition consists of three well-defined regimes identified with increasing electrostatic interaction strength. In the first regime, the size of the whole chain decreases, while the size of the individual blocks increases slightly with $l_B$, reaches a maximum value, and starts to decrease. The variation of the size of the individual blocks in this regime is very weak. For the diblock chain presented in Figure 1, the ratio of the peak value of $R_{g,blk}$ at $l_B \approx \sigma/8$ to the radius of gyration of the block without electrostatic interactions (at $l_B = 0$) is about 1.04. This implies that in this regime the size of the whole chain decreases due to the overlap of the two blocks (chain folding), while the size of each block slightly increases due to self-repulsion of its charges, similar to the onset of elongation of a polyelectrolyte chain. In the second regime, the average sizes of the whole chain and the individual blocks are equal to each other, reflecting the collapse of the chain into a globule. The third regime is characterized by the ionic binding of oppositely charged monomers due to the strong electrostatic attraction between them. The typical conformations of the chain in different regimes are presented in Figure 2 by the snapshots at different values of the Bjerrum length $l_B$.

The conformational properties of a diblock polyampholyte in the globular state can be analyzed using the concept of electrostatic blobs.[49,50] On length scales smaller than the electrostatic blob size, $\xi_e$, the chain statistics are almost unperturbed by the electrostatic interactions. This electrostatic blob size, $\xi_e$, and the corresponding number of monomers, $g_e$, in it are determined by the balance between the electrostatic and thermal parts of the free energy:

$$l_B k_B T (f g_e)^2/\xi_e \approx k_B T \tag{8}$$

where $\xi_e$ follows the scaling law of a neutral chain

$$\xi_e \approx g_e{}^{\nu}\sigma \tag{9}$$

and the value of the scaling exponent $\nu$ is 0.5 in a Θ-solvent and 0.588 in a good solvent. Equations 7 and 8 lead to the scaling dependences of $\xi_e$ and $g_e$ on the interaction parameter $l_B f^2/\sigma$

$$\xi_e \approx \sigma (l_B f^2/\sigma)^{-\nu/(2-\nu)} \tag{10}$$

$$g_e \approx (l_B f^2/\sigma)^{-1/(2-\nu)} \tag{11}$$

If the total number of monomers $N$ in a charged polymer is smaller than $g_e$, its conformation is almost unperturbed and the chain size scales as $R_{g0} \propto N^{\nu}\sigma$ (eq 9). However, if there are many electrostatic blobs per chain, $N \gg g_e$, that can be rewritten as

$$N^{2-\nu} l_B f^2/\sigma \approx l_B (f N)^2/R_{g0} \gg 1 \tag{12}$$

the electrostatic interactions play a dominant role in determining the chain conformation at length scale larger than the electrostatic blob size $\xi_e$. To verify this prediction, the relative reduction of the total chain size, $R_g/R_{g0}$, is presented in Figure 3 as a function of the universal interaction parameter $l_B(f N)^2/R_{g0}$ for different diblock polyampholytes in (a) good solvent and (b) Θ-solvent conditions. In each case the data points are found to collapse onto a universal curve. The results indicate that the scaling parameter controlling the onset of the conformational changes is correctly predicted by eq 12. Starting from the value of $R_g/R_{g0} = 1$ for uncharged chains, these universal curves cover the entire parameter range of the first (folding) and the second (globular) regimes in the coil−globule transition of diblock polyampholytes. The average radii of gyration of the individual blocks also exhibit universal behavior, as can be seen from the lower curves in Figure 3 for the rescaled block sizes, $R_{g,blk}/R_{g0}$. The ratio of block size to the unperturbed chain size, $R_{g,blk}/R_{g0}$, remains close to its uncharged chain value $2^{-\nu}$ for weak electrostatic interactions ($N^{2-\nu} l_B f^2/\sigma < 1$) and has a slight increase in the folding regime of the diblock polyampholyte. In the second (globular) regime of the conformational transition, the universal curve of the individual block size coincides with the universal curve for the size of the whole chain. The results in the strong association regime are not shown in Figure 3. In that case the variation of the chain size does not follow the same scaling behavior due to the strong ionic binding between oppositely charged monomers. The simulation results of Imbert et al. on single diblock polyampholytes[28] and Winkler et al. on pairs of oppositely charged polyelectrolytes[14] have also revealed a universal behavior of $R_g/N^{\nu}$ as a function of $N^{2-\nu} l_B/\sigma$ for the case of charge fraction $f = 1$ and good solvent condition.

Figure 4 shows the diagram of conformational states of a diblock polyampholyte in the Bjerrum length, $l_B$, and charge fraction, $f$, plane. Different conformational regimes and the transitions between them are discussed in details below.

**3.1. Folding Regime.**[51] At the onset of this regime the electrostatic blob size $\xi_e$ is on the same order of magnitude as the size of the whole chain. The boundary between the folding regime and the unperturbed chain (coil state) is defined by

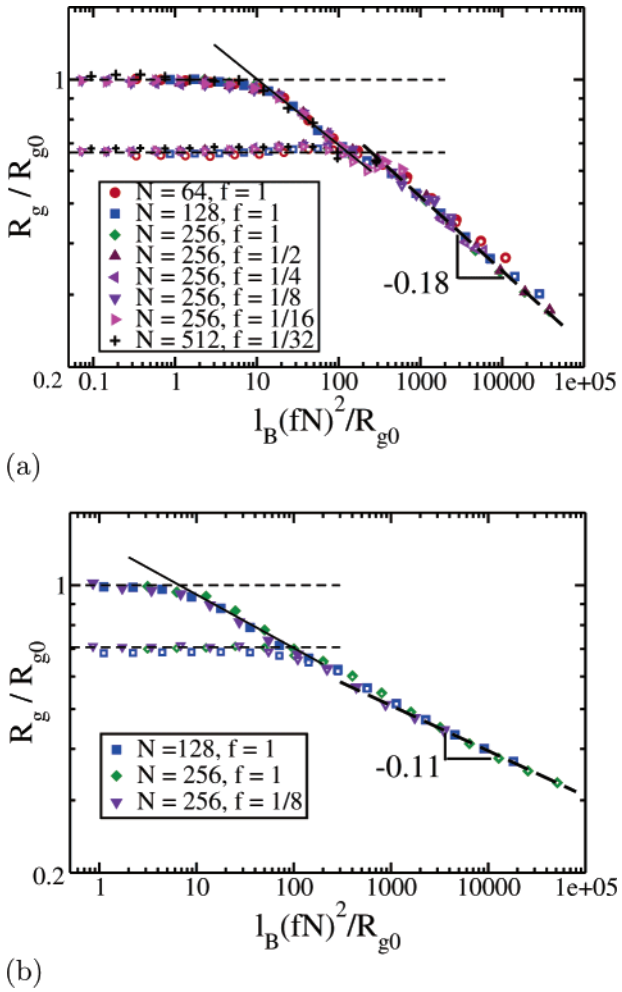


**Figure 3.** Normalized root-mean-square radii of gyration of the diblock polyampholyte chains (solid symbols) and of the individual blocks (open symbols) as a function of the universal interaction parameter in (a) good and (b) Θ-solvent conditions. The horizontal thin dashed lines correspond to the radii of gyration of the uncharged chain (upper) and of the uncharged individual blocks (lower), respectively. The solid lines are the power-law fit to the data points in the central 50% part of the folding regime. The thick dashed lines are the power law predictions of the scaling theory (eq 19) with the exponents indicated in the corresponding figures.

eq 12, which can be rewritten as

$$l_B^{fold} = C_f f^{-2} N^{\nu-2} \sigma \tag{13}$$

The numerical coefficients $C_f = 4.7$ in a good solvent and $C_f = 3.1$ in a Θ-solvent are determined from our simulation data by a power law fit of $R_g/R_{g0}$ as a function of the universal interaction parameter $l_B(fN)^2/R_{g0}$ in the folding regime (see solid lines in Figure 3 corresponding to the best fit to central half of the data points in the region $2^{-\nu} \le R_g/R_{g0} \le 1$ for both solvent conditions), and using our simulation results of $R_{g0} \approx 0.46N^{\nu}\sigma$ in both solvents. The onset of the folding regime obtained from the intersection of the power law fit with the short dashed line at $R_g/R_{g0} = 1$ is at $l_B(fN)^2/R_{g0} = 10.2 \pm 1.7$ in a good solvent and $l_B(fN)^2/R_{g0} = 6.8 \pm 1.2$ in a Θ-solvent[52] (with the chain size at the onset of the folding regime $R_g \approx 0.95R_{g0}$). The crossover boundary between the coil and the folding regime (eq 13) calculated for $N = 256$ in a good solvent is presented by line I (thin solid line) in Figure 4.

The folding process of a diblock polyampholyte can be described by a simple mean-field model. The diblock chain can be represented by two oppositely charged objects of identical

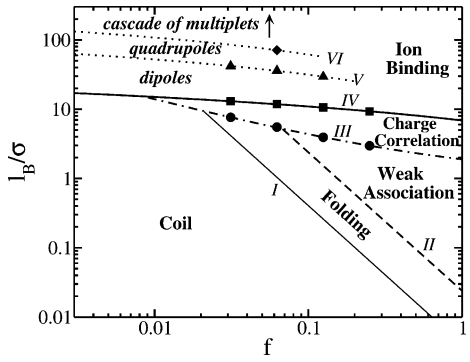


**Figure 4.** Diagram of conformational states of a diblock polyampholyte in the Bjerrum length, $l_B$, and charge fraction, $f$, plane in a good solvent. The lower boundary of the folding regime (thin solid line I) and the lower boundary of the weak association regime (dashed line II) are calculated for the degree of polymerization $N = 256$. The upper boundary of the weak association regime (dashed−dotted line III), the lower boundary of the ion binding regime (thick solid line IV), and the cascade of multiplet transitions (dotted lines V, VI, ...) are numerical fits for the simulation results obtained for diblock polyampholytes with charge fraction $f \le 1/4$.

size with their centers of mass linked by an entropic spring, as sketched in the inset of Figure 5a. The electrostatic attraction energy between the two oppositely charged objects and the elastic energy of the spring are balanced by the short-range repulsive energy between monomers in the overlapping region of the blocks (shaded area in the inset of Figure 5a). The average distance between the centers of mass of the two objects (blocks), $r_{cm}$, and consequently the average radius of gyration of the model system (representing that of a diblock polyampholyte), $R_g$, is determined by the total free energy of the model system at different values of the Bjerrum length $l_B$. This free energy depends on the monomer distribution of each polyampholyte block.

We have examined the radial density profile $n(r)$ that is defined as the average number density of monomers measured at a distance $r$ from the center of mass of the corresponding block. This density profile $n(r)$ of the individual blocks for the diblock polyampholyte with $N = 256$ monomers and charge fraction $f = 1/4$ at different values of $l_B$ in the folding regime is plotted in Figure 6. It demonstrates that the monomer density profile $n(r)$ of an uncharged block is well approximated by the Gaussian distribution

$$n(r) = \frac{N/2}{(\pi\alpha^2)^{3/2}} \exp(-r^2/\alpha^2) \tag{14}$$

with $\alpha^2 = 2R_{g0,blk}^2/3$ (solid line in Figure 6). However, the curves for the density distribution $n(r)$ flatten at small values of $r$ with increasing Bjerrum length $l_B$. The appearance of the plateau in the monomer density profile of the blocks (and of the whole chain) indicates the crossover from a distribution well approximated by a Gaussian function in the coil regime to the uniform density distribution in a diblock polyampholyte globule.

We have performed mean-field theoretical calculations using both the uniform and Gaussian monomer distributions, corresponding to the limiting monomer density profiles inside the blocks in the folding regime. In the case of a uniform distribution, the two individual blocks are represented by two uniformly charged spheres with the radius $R_{sp} = (5/3)^{1/2}R_{g0,blk}$ which ensures that the radius of gyration of each sphere is equal to that of each uncharged block. Since the average block size is almost unchanged from its neutral value $R_{g0,blk}$ in the folding regime, the radius of the spheres is also fixed in the calculations. When the Gaussian monomer distribution is used, the density

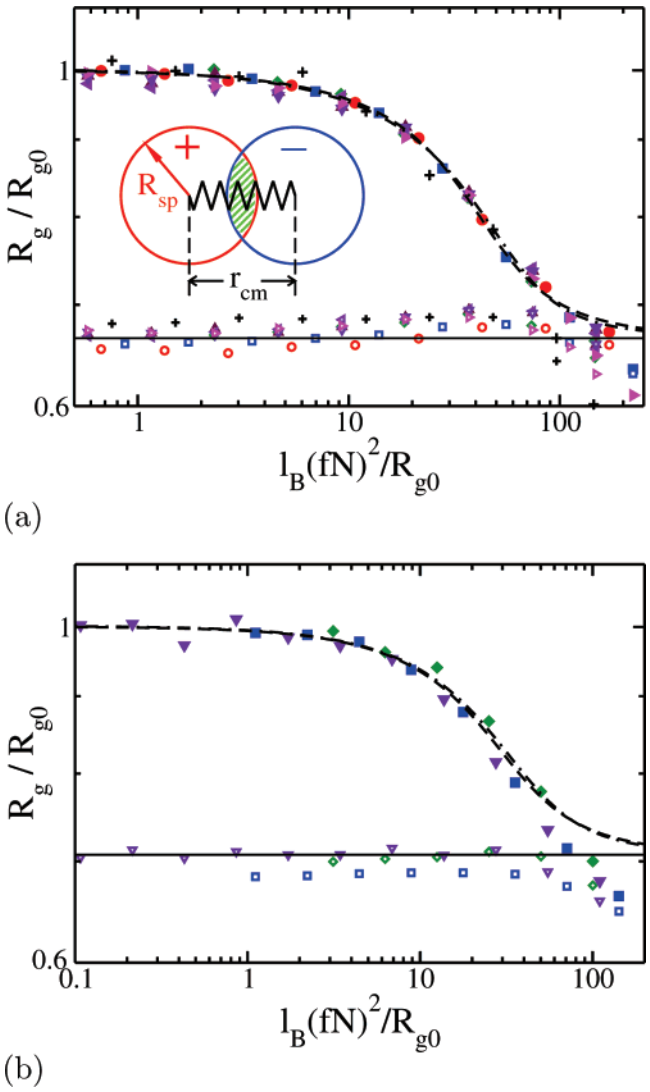


**Figure 5.** Comparison of the theoretical predictions for the radii of gyration of the diblock polyampholytes in the folding regime obtained using the uniform (dashed lines) and Gaussian (dashed−dotted lines) monomer distribution models for (a) good and (b) Θ-solvent conditions. The simulation results (symbols) have the same notations as in Figure 3. The horizontal thin solid lines are the normalized radii of gyration of individual blocks used in the theoretical calculations.

profile of eq 14 is employed for each block. The details of the theoretical calculations are presented in the Appendix. The numerical results on the rescaled radius of gyration, $R_g/R_{g0}$, are shown as dashed lines for uniform distribution and dashed−dotted lines for Gaussian distribution in Figure 5. It can be seen that the calculations using the two different limiting density profiles provide very similar numerical results. Good agreement of theoretical predictions with simulation results is obtained in both good- and Θ-solvent conditions. This indicates that the essential feature of the folding regime is the electrostatically driven overlap of the two blocks. The small quantitative discrepancy between the theoretical and simulation results at larger values of the interaction parameter is due to the fact that charge density fluctuations are neglected in the mean-field model.

As shown in Figure 5, the electrostatic interaction parameter $l_B(fN)^2/R_{g0}$ has to increase by more than one order of magnitude in order to fold a diblock polyampholyte from its unperturbed coil state to the size of an individual block. The reason for this unexpectedly wide folding regime is the effective charge neutralization in the overlapping region of the two

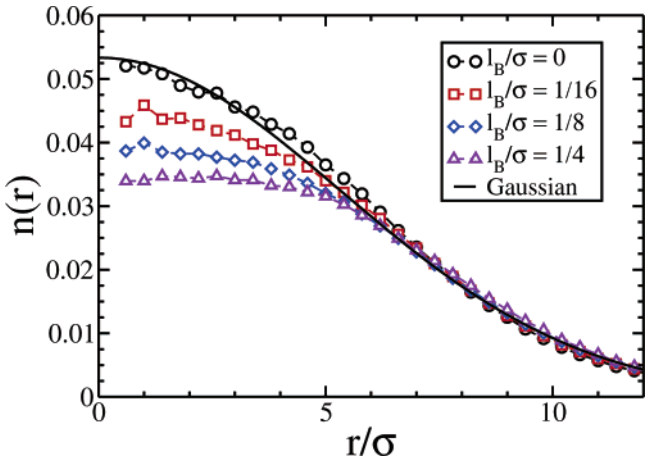


**Figure 6.** Number density $n(r)$ of monomers in an individual block of the diblock polyampholyte with $N = 256$ and $f = 1/4$ in good solvent condition as a function of the distance $r$ from the center of mass of the block. The symbols are simulation results at different values of the Bjerrum length $l_B$ averaged over the two individual blocks. The solid line is the Gaussian function (eq 14) with the radius of gyration of the uncharged block $R_{g0,blk} = 9.25\sigma$.

charged blocks (the mean-field charge density is zero in this region). As a result, the electrostatic attraction force, $dF^{el}/dr_{cm}$, between the two oppositely charged blocks decreases with the decrease of their center-to-center distance $r_{cm}$ at small separations for a fixed value of the electrostatic interaction parameter, in contrast to the increasing electrostatic force between two point charges. The uniform monomer distribution model estimates that the attractive force between the two blocks is about $0.1l_Bk_BT(fN)^2/R_{g0}^2$ near the globule state (at $R_g \approx 1.03R_{g0,blk}$) in a good solvent (see eq A10). Balancing this force with the two-body repulsive force $\approx 6.6k_BT/R_{g0}$ (see eq A5) at the globular state reveals that a value of $l_B(fN)^2/R_{g0}$ on the order of 100 is required in order to fold a diblock polyampholyte.

The mean-field model used in this section ignores the correlated charge density fluctuations in the system. This is reasonable since the fluctuation-induced electrostatic attraction energy is less than or comparable to $k_BT$ in almost the entire folding regime, except for the region close to the upper boundary of this regime where the two individual blocks nearly completely overlap with each other. In that case the fluctuation-induced attraction energy is of the order of several $k_BT$, while the mean-field electrostatic energy almost vanishes. When the system enters the weak association regime, the fluctuation-induced attraction energy dominates the total electrostatic energy, as discussed in the next subsection. The fact that we neglected charge density fluctuations in the mean-field calculations leads to the underestimation of the electrostatic attraction energy near the end of the folding regime and consequently results in the overestimation of the chain size in comparison with the simulation results at high values of the interaction parameter.

The folding regime can only be observed in dilute solutions of diblock polyampholytes. At higher concentrations, the interchain attraction leads to aggregation of chains into complexes in the range of interaction parameter corresponding to the folding regime.

**3.2. Weak Association Regime.** The globular state of a symmetric diblock polyampholyte starts when the size of the whole chain $R_g$ coincides with the size of the individual blocks $R_{g,blk}$. The universal interaction parameter at the onset of the globular state is determined from the intersection between the fitting curve (solid line) for the data points in the central part of the folding regime and the short dashed line at $R_g/R_{g0} = 2^{-\nu}$

in Figure 3. It is found to be at $l_B^{weak}(fN)^2/R_{g0} = 130 \pm 10$ in a good solvent and $96 \pm 5$ in a Θ-solvent, respectively. This boundary between the folding and globular (weak association) regimes can be written as

$$l_B^{weak} = C_w f^{-2} N^{\nu-2} \sigma \tag{15}$$

where the coefficient $C_w \approx 60$ in a good solvent and $C_w \approx 44$ in a Θ-solvent were obtained using $R_{g0} \approx 0.46 N^{\nu}\sigma$ in both solvents. This boundary (eq 15) calculated for $N = 256$ in a good solvent is presented by line II (dashed line) in Figure 4. Note that line II is parallel to line I because eqs 13 and 15 differ only by the numerical factor.

The electrostatic blob size $\xi_e$ in the globular state is smaller than the globule size $R_g$ but is larger than the average distance between a pair of adjacent charged monomers along each block (the average size of the neutral spacer, $\sim f^{-\nu}\sigma$). This regime is called the weak association regime because the average Coulomb energy per charge is less than $k_BT$.

We demonstrate below that the physical properties of diblock polyampholytes in the weak association regime can be well described by the "scrambled egg" model.[26,27] In this model the fluctuation-induced electrostatic attraction is the driving force for the collapse of the flexible diblock polyampholytes. The free energy can be calculated in a way similar to that of a Debye−Hückel electrolyte solution.[24,25,37,53,54] The structure of a collapsed flexible diblock polyampholyte as well as of a complex formed by oppositely charged flexible polyelectrolytes can be represented by a compact packing of the so-called "complexation blobs" of size $\xi_c$.[24,53] At length scales smaller than $\xi_c$ the electrostatic attraction induced by charge density fluctuations is smaller than the thermal energy $k_BT$, but at length scales larger than $\xi_c$ electrostatic attraction is larger than the thermal energy and dominates the properties of the globule. The electrostatic attraction energy between two neighboring oppositely charged blobs is on the order of $k_BT$. This attraction is balanced by the steric repulsion between the two blobs which is also on the order of $k_BT$. It is easy to see that the complexation blobs in block polyampholytes and in complexes of oppositely charged polyelectrolytes are comparable in size to the electrostatic blobs defined in eq 8. Hereafter, we use the term of electrostatic blob for both of them.

The physical picture of weakly associated globules is a dense packing of electrostatic blobs where each blob is predominantly surrounded by oppositely charged blobs. The size of the diblock polyampholyte globules can thus be calculated to be[24,25]

$$R_g \approx \xi_e \left(\frac{N}{g_e}\right)^{1/3} \approx \sigma N^{1/3} (l_B f^2/\sigma)^{(1-3\nu)/[3(2-\nu)]} \tag{16}$$

where $\xi_e$ and $g_e$ are the electrostatic blob size and the number of monomers in it, respectively (eqs 10 and 11). The equilibrium volume fraction of monomers, $\phi$, inside the globule is thus the same as the volume fraction inside an electrostatic blob

$$\phi \approx \frac{N\sigma^3}{R_g^3} \approx \frac{g_e\sigma^3}{\xi_e^3} \approx (l_B f^2/\sigma)^{(3\nu-1)/(2-\nu)} \tag{17}$$

Equation 16 can be written as

$$\frac{R_g}{N^{\nu}\sigma} \approx (N^{2-\nu} l_B f^2/\sigma)^{(1-3\nu)/[3(2-\nu)]} \tag{18}$$

or equivalently as

$$\frac{R_g}{R_{g0}} \approx [l_B (fN)^2/R_{g0}]^{(1-3\nu)/[3(2-\nu)]} \tag{19}$$

The exponent on the right-hand side of eqs 18 and 19 is about −0.18 in a good solvent ($\nu = 0.588$) and −0.11 in a Θ-solvent ($\nu = 0.5$). Figure 3 shows that the predictions of the scaling calculations agree very well with our simulation results in both solvent conditions. This result confirms the theoretical assumption that the fluctuation-induced electrostatic attraction is the driving force for the collapse of the diblock polyampholytes in the weak association regime.[24,25]

The correlation length in the weak association regime can be numerically estimated by calculating the average distance between two nearest oppositely charged monomers

$$\xi_{+-}^{1st} = \left\langle \frac{2}{fN} \sum_{k=1}^{fN/2} (\mathbf{r}_k - \mathbf{r}_k^{near})^2 \right\rangle^{1/2} \tag{20}$$

Here $\mathbf{r}_k$ is the position of charged monomer $k$, and $\mathbf{r}_k^{near}$ is the location of the oppositely charged monomer nearest to monomer $k$. Since neighboring electrostatic blobs are typically oppositely charged, the average minimum distance between oppositely charged monomers is on the order of the electrostatic blob size $\xi_e$, i.e., $\xi_{+-}^{1st} \approx \xi_e$. Similarly, we have calculated the average distances between two nearest positive charges, $\xi_{++}^{1st}$, as well as between two nearest negative charges, $\xi_{--}^{1st}$. Since the two blocks are symmetrical, $\xi_{++}^{1st}$ is equal to $\xi_{--}^{1st}$ in all cases, and thus we only show the average distance between two nearest same-sign charges $\xi_{++(--)}^{1st} = (\xi_{++}^{1st} + \xi_{--}^{1st})/2$. In the absence of strong binding $\xi_{++(--)}^{1st}$ is the average distance between two adjacent charges along each block. It can be estimated as the average size of the neutral spacer between two adjacent charges along the block or as the average size of the chain section containing $f^{-1}$ monomers

$$\xi_{++(--)}^{1st} \approx \sigma f^{-\nu} \tag{21}$$

Figure 7 shows the average distance between two nearest oppositely charged monomers, $\xi_{+-}^{1st}$, and between two nearest charged monomers of same sign, $\xi_{++(--)}^{1st}$, as a function of the Bjerrum length determined from our MD simulations of a diblock polyampholyte with $N = 256$ monomers and charge fraction $f = 1/8$ in a good solvent. The distance between nearest charges with the same sign $\xi_{++(--)}^{1st}$ remains close to the average size of neutral spacers ($\approx f^{-\nu}\sigma$) at smaller Bjerrum length $l_B$ and slightly increases at larger $l_B$ due to electrostatic repulsions along each block. For example, in Figure 7 the peak value of $\xi_{++(--)}^{1st}$ at $l_B \approx 4\sigma$ is about 1.06 times $\xi_{++(--)}^{1st}$ at $l_B = 0$. The decrease of the distance between nearest oppositely charged monomers $\xi_{+-}^{1st}$ with the Bjerrum length $l_B$ follows the same scaling law as the electrostatic blob size in a good solvent $\xi_e \sim l_B^{-0.42}$ (see eq 10) in the weak association regime. It verifies the close packing of electrostatic blobs in the collapsed globule. Figure 8 shows the universal plot of the electrostatic blob size (determined in simulations as $\xi_{+-}^{1st}$) as a function of $l_B f^2$ for the diblock chains in a good solvent with fixed degree of polymerization $N = 256$ but different charge fractions. The scaling behavior of the correlation length $\xi_{+-}^{1st}$ for globules formed in a Θ-solvent in the weak association regime also follows the same scaling law as the electrostatic blob size, $\xi_e \sim l_B^{-1/3}$.

The weak association regime ends when there is on average only one charge in each electrostatic blob. Since the average number of monomers in the chain section containing a single

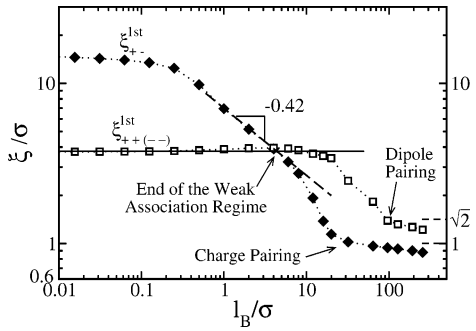


**Figure 7.** Root-mean-square average distance between the nearest oppositely charged monomers, $\xi^{1st}_{+-}$ (solid diamonds), and between the nearest monomers with the same sign of charges, $\xi^{1st}_{++(--)}$ (open squares), as functions of the Bjerrum length $l_B$ for the diblock chain with $N = 256$ and $f = 1/8$ in a good solvent condition. The dashed line is the theoretical prediction for the electrostatic blob size (eq 10), and the horizontal line is the size of the uncharged spacer.

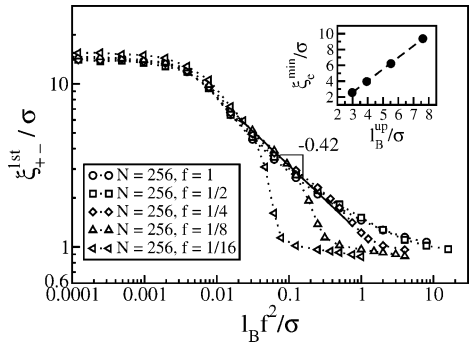


**Figure 8.** Root-mean-square average distance $\xi^{1st}_{+-}$ between the nearest oppositely charged monomers as a function of $l_B f^2/\sigma$ for the diblock polyampholytes with a fixed chain length $N = 256$ and different charge fractions $f$ in a good solvent condition. The dashed line is the theoretical prediction for the electrostatic blob size (eq 10). The inset graph shows the values of $l^{up}_B$ and $\xi^{min}_e$ for cases of $f \leq 1/4$ determined from the intersection point of the $\xi^{1st}_{+-}$ and $\xi^{1st}_{++(--)}$ curves as depicted in Figure 7.

charge is $f^{-1}$, the average size of the minimum possible electrostatic blob, $\xi^{min}_e$, is given by

$$\xi^{min}_e \approx f^{-\nu}\sigma \tag{22}$$

Substituting eq 22 into eq 10, we obtain the upper boundary of the weak association regime

$$l^{up}_B \approx f^{-\nu}\sigma \approx \xi^{min}_e \tag{23}$$

The Bjerrum length $l^{up}_B$ at the upper boundary of the weak association regime is on the same order of magnitude as the minimum electrostatic blob size $\xi^{min}_e$ because in this case the interaction energy between two neighboring electrostatic blobs ($k_BT$) is equal to that between two neighboring charges. The value of $l^{up}_B$ is independent of the degree of polymerization of the diblock chains. In Figure 7, this upper boundary is defined by the intersection point between the $\xi^{1st}_{+-}(l_B)$ and $\xi^{1st}_{++(--)}(l_B)$ curves [note that in this regime $\xi^{1st}_{++(--)}(l_B) \approx f^{-\nu}\sigma$]. The simulation results of the upper boundary of the weak association regime and the numerical fit to them ($l^{up}_B = 0.86f^{-\nu} + 1.03$) are presented in Figure 4 by circles and line III (dashed−dotted line), respectively.

In the inset graph of Figure 8, we present the simulation results of the minimal electrostatic blob size, $\xi^{min}_e$, as a function of the Bjerrum length, $l^{up}_B$, at the upper boundary of the weak association regime for the diblock chains with $f \leq 1/4$. It clearly reveals the linear proportionality between $\xi^{min}_e$ and $l^{up}_B$ (linear fit to simulation data is $\xi^{min}_e \approx 1.44l^{up}_B - 1.7\sigma$) as predicted by eq 23. The values of $l^{up}_B$ and $\xi^{min}_e$ obtained for diblock polyampholytes with very high charge fractions $f \geq 1/2$ are somewhat larger than the theoretical predictions because in these cases the neutral spacer consists of very few monomers (1 for $f = 1/2$ and 0 for $f = 1$). The minimum electrostatic blob size $\xi^{min}_e$ in these highly charged chains is on the order of the monomer size $\sigma$. It means that the monomers are densely packed in the globules for the Bjerrum length $l_B$ near the upper boundary of the weak association regime. The steric repulsion between the monomers hinders further contraction of the globules at higher values of $l_B$. The average distance between the nearest oppositely charged monomers, $\xi^{1st}_{+-}$, for chains with $f \geq 1/2$ decreases with Bjerrum length, $l_B$, at a rate slower than that predicted by the scaling law of eq 10 (see Figure 8), resulting in the larger values of $l^{up}_B$ and $\xi^{min}_e$.

The width of the weak association regime, $l^{up}_B/l^{weak}_B \approx (fN)^{2-\nu}/C_w$ (see eqs 15 and 23) increases with the total number of charges, $fN$, along the chain. This can be seen in Figure 8 where the width of the weak association regime is reflected by the region in which the $\xi^{1st}_{+-}$ curve follows the scaling law of eq 10 for the electrostatic blob size. The width of this regime for the diblock chain with $N = 256$ monomers is about 2 decades for $f = 1$ but is reduced to about 1 decade for $f = 1/4$ and almost disappears for $f = 1/16$. Figure 4 also shows that at fixed $N$ the width of the weak association regime increases with the charge fraction $f$ of the diblock chain. Since the lower boundary of the weak association regime $l^{weak}_B$ (eq 15) shifts to lower values of $l_B$ as the degree of polymerization $N$ is increased, the width of this regime increases at a fixed value of $f$ with increasing $N$.

At higher Bjerrum length ($l_B > l^{up}_B$), the average distance between a pair of nearest oppositely charged monomers, $\xi^{1st}_{+-}$, is smaller than the minimum electrostatic blob size, $\xi^{min}_e$ (see Figure 7), and the Coulomb energy between these two charges is larger than $k_BT$. The oppositely charged monomers are beginning to be strongly correlated with each other, but the electrostatic gain for binding a pair of opposite charges into a dipole is still lower than the energetic and entropic cost associated with dipole formation. In this charge correlation region between lines III and IV in Figure 4, the probability for a charged monomer to be bound into a dipole is smaller than that for it to be an isolated charge. For a diblock polyampholyte with $N = 256$ monomers and charge fraction $f = 1/4$, the Bjerrum length in the charge correlation region is in the interval of $3\sigma \leq l_B \leq 9.4\sigma$. The system enters the ion binding regime when a charged monomer has a higher probability to be in a dipole than to stay unbound. The transition to the ion binding regime is discussed in the next subsection.

It should be noted that although the above scaling calculations are made for a single symmetric diblock polyampholyte chain, they could also be applied to the complexation (micellization) in solutions of diblock polyampholytes.[24,25] More importantly, the complexation of oppositely charged polyelectrolytes[15,55] can also be well understood by the "scrambled egg" model because there is no qualitative difference between the physical properties inside the complexes formed by diblock polyampholytes and the complexes formed by oppositely charged polyelectrolytes.

### 3.3. Ion Binding Regime.

**a. Diblock Polyampholyte.** Ion binding between oppositely charged monomers takes place if the electrostatic attraction

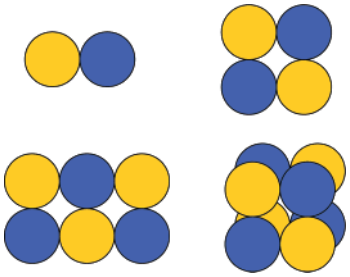

**Figure 9.** Ground state of the multiplets formed by oppositely charged particles: dipole ($s = 2$), quadrupole ($s = 4$), hexapole ($s = 6$), and octupole ($s = 8$). The circles filled with two different colors correspond to particles with charges of opposite signs.

energy is strong enough to overcome the entropic penalty as well as steric repulsion between neutral chain sections. The average distance $\xi_{+-}^{1st}$ between nearest oppositely charged monomers sharply decreases with the Bjerrum length $l_B$ and approaches a saturation value on the order of the monomer size $\sigma$ (see Figures 7 and 8), indicating the charge pair (dipole) formation. These dipoles further aggregate into higher order multiplets such as quadrupoles, hexapoles, and octupoles, at higher values of Bjerrum length $l_B$. There is a cascade of multiplet formation transitions with increasing strength of the electrostatic interactions. Since the electrostatic attraction energy per charge in the multiplets is much larger than the thermal energy $k_BT$, these aggregates are in the strong association regime.

The ground state of a multiplet formed by oppositely charged particles is defined by the geometric arrangement of these particles which minimizes the total electrostatic energy. Figure 9 demonstrates the ground states of the multiplets formed by $s = 2$ (dipole), 4 (quadrupole), 6 (hexapole), and 8 (octupole) charged particles. The well-defined geometry of these multiplets indicates that the multiplet formation in charged polymer systems can be analyzed by studying average distances of a charged monomer with its various neighbors (first, second, third, and so forth) with either opposite or same sign of charge. We denote these various distances by $\xi_{+-}^{ith}$ and $\xi_{++(--)}^{ith}$ and use them as indicators signaling different stages of the multiplet formation process. Following Figure 9, a positively charged monomer has one (first) nearest negatively charged neighbor in a dipole state with $\xi_{+-}^{1st} \approx \sigma$. In a quadrupole it has two nearest negatively charged neighbors at $\xi_{+-}^{1st} \approx \xi_{+-}^{2nd} \approx \sigma$ and one nearest positively charged neighbor at $\xi_{++}^{1st} \approx \sqrt{2}\sigma$, while in a well-organized octupole with cubic geometry it has three negative charges at the nearest distance, $\xi_{+-}^{1st} \approx \xi_{+-}^{2nd} \approx \xi_{+-}^{3rd} \approx \sigma$, three positive charges at the distance, $\xi_{++}^{1st} \approx \xi_{++}^{2nd} \approx \xi_{++}^{3rd} \approx \sqrt{2}\sigma$, and one negative charge at the opposite corner of the cube, $\xi_{+-}^{4th} \approx \sqrt{3}\sigma$.

Figure 10 presents the simulation results on the distances between different pairs of charged monomers $\xi_{+-}^{ith}$ and $\xi_{++(--)}^{ith}$ as a function of the Bjerrum length $l_B$ for the diblock polyampholyte of $N = 256$ and $f = 1/16$ in a good solvent. The stepwise decrease of the distances between charges $\xi_{+-}^{ith}$ and $\xi_{++(--)}^{ith}$ and their saturation at different $l_B$ values clearly reveal a cascade of multiplet formation transitions from isolated charged monomers to dipoles, quadrupole, and higher order multiplets. The formation of multiplets of different sizes can be seen in Figure 11, which presents the snapshots of the diblock polymer at different values of Bjerrum length $l_B$.

The average distance between nearest opposite charges $\xi_{+-}^{1st}$ (solid circles) sharply decreases with increasing $l_B$ in the charge correlation regime above the intersection of curves $\xi_{+-}^{1st}(l_B)$ and

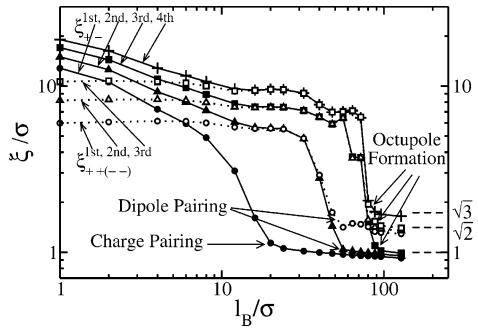


**Figure 10.** Root-mean-square average distances between charged monomers with their first (circles), second (triangles), third (squares) and fourth (crosses) nearest oppositely (solid symbols) and same-sign (open symbols) charged neighbors as a function of the Bjerrum length $l_B$ for the diblock polyampholyte with $N = 256$ and $f = 1/16$ in good solvent condition. The arrows are used to indicate the points of different multiplet formation.

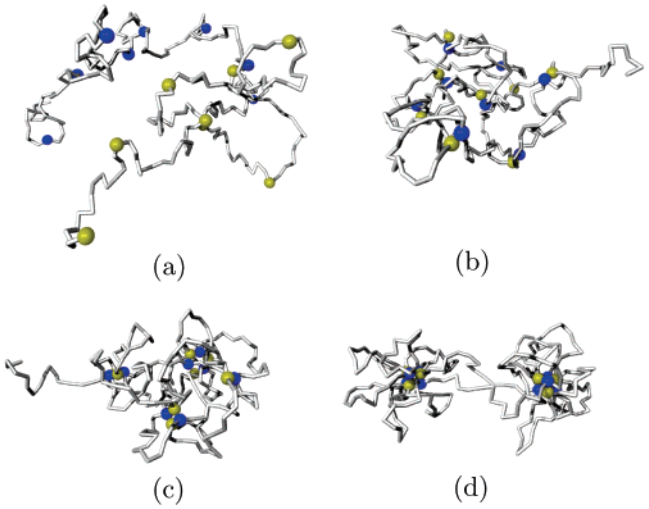


**Figure 11.** Typical conformations of the diblock polyampholyte chain with $N = 256$ and $f = 1/16$ in a good solvent condition at different Bjerrum lengths: (a) $l_B = 4\sigma$; (b) $l_B = 20\sigma$; (c) $l_B = 48\sigma$; (d) $l_B = 96\sigma$. Oppositely charged monomers are presented as spheres with different colors.

$\xi_{++(--)}^{1st}(l_B)$ (open circles) (see Figure 10), indicating the onset of dipole formation. When the Bjerrum length increases to $l_B \approx 20\sigma$, $\xi_{+-}^{1st}$ approaches the value of $\sigma$. It means that almost all charged monomers are in dipoles (see Figure 11b). Following the dipole formation, the values of $\xi_{+-}^{2nd}$ (solid triangles) and $\xi_{++(--)}^{1st}$ coincide, since both of them now measure the average distance between nearest dipoles. A further increase of the strength of the electrostatic interactions leads to the pairing of the dipoles, and correspondingly the distances $\xi_{+-}^{2nd}$ and $\xi_{++(--)}^{1st}$ decrease sharply with increasing Bjerrum length. At $l_B \approx 48\sigma$, the two distances separate from each other, reflecting the onset of the dipole pairing (quadrupole formation). The snapshot in Figure 11c obtained at $l_B = 48\sigma$ shows the coexistence of two quadrupoles with one dipole and one hexapole. When the Bjerrum length is increased to $l_B \approx 60\sigma$, we have $\xi_{+-}^{2nd} \approx \xi_{+-}^{1st} \approx \sigma$ and $\xi_{++(--)}^{1st} \approx \sqrt{2}\sigma$. Almost all dipoles are bound forming quadrupoles and even some higher order multiplets (e.g., hexapoles). The charge pairing and dipole pairing stages can also be seen in Figure 7 for the diblock polyampholyte with degree of polymerization $N = 256$ and charge fraction $f = 1/8$.

In the ion binding regime, the distances $\xi_{+-}^{3rd}$ (solid squares) and $\xi_{++(--)}^{2nd}$ (open triangles) measure the average separation

between a dipole and its second nearest neighbor dipole. Above the dipole binding transition these distances measure the average separation between two nearest quadrupoles. These distances ($\xi_{+-}^{3rd}$ and $\xi_{++(--)}^{2nd}$) coincide with each other in the region where dipoles and quadrupoles dominate over the multiplets. After the dipole binding transition, the two distances decrease at stronger electrostatic interactions and their values separate at $l_B \approx 80\sigma$. The similar argument applies to the distances $\xi_{+-}^{4th}$ (cross) and $\xi_{++(--)}^{3rd}$ (open squares). The typical signature of octupole formation ($\xi_{+-}^{1st,2nd,3rd} \approx \sigma$, $\xi_{++}^{1st,2nd,3rd}{}_{(--)} \approx \sqrt{2}\sigma$, and $\xi_{+-}^{4th} \approx \sqrt{3}\sigma$) is reached at Bjerrum length $l_B \approx 90\sigma$, above which octupoles are more numerous than other types of multiplets in the system. Figure 11d shows the formation of two well-organized octupoles at Bjerrum length $l_B = 96\sigma$. Although the formation of hexapoles has been observed in our simulations (e.g, see Figure 11c), the typical values of $\xi_{+-}^{3rd} \approx 2\sigma$ and $\xi_{++(--)}^{2nd} \approx \sqrt{5}\sigma$ expected for the ground state of hexapoles are not clearly visible in Figure 10. A possible explanation is that the electrostatic energy of the ground state of a hexapole shown in Figure 9 is within $k_BT$ of the energy of a ringlike hexagonal geometry with alternating sequence of the oppositely charged monomers. In simulations we observed transformations of hexapoles between these two different geometries due to thermal fluctuations, and the resulting average values of $\xi_{+-}^{3rd}$ and $\xi_{++(--)}^{2nd}$ differ from those expected for the ground state of a hexapole. The existence of hexapoles as well as transitions between different multiplets is clearly determined by the following cluster analysis.

**b. Cluster Analysis.** An alternative way of describing the cascade of multiplet formations is to calculate the probability $P_s$ for a charged monomer to be a part of a multiplet (cluster) consisting of $s$ charged monomers[56−58]

$$P_s = \langle sN_s \rangle / \sum_s (sN_s) \tag{24}$$

where $N_s$ is the number of clusters of size $s$ and $\sum_s(sN_s)$ ($= fN$) is the total number of charged monomers in the diblock polyampholyte. Two oppositely charged monomers are defined to be part of the same cluster if the electrostatic attraction energy between them is stronger than $-l_Bk_BT/(1.5\sigma)$ or, equivalently, the distance between their centers is smaller than the cutoff distance $r_{cut} = 1.5\sigma$. In the case of low charge fractions, this energetic criterion provides the same results as the geometric criterion where all charged monomers at a distance smaller than $r_{cut}$ are taken to be in the same cluster. But in case of high charge fractions (e.g., $f \geq 1/2$), the use of the energetic criterion avoids the problem of grouping all adjacent same-sign charged monomers along the block into a same cluster due to their spatial proximity. The results of the cluster analysis exhibit a weak dependence on the cutoff distance $r_{cut}$ as its value was changed from $\sigma$ to $1.5\sigma$, which is consistent with ref 57.

Figure 12 presents the simulation results for the probability, $P_s$, of a charged monomer to be a part of a charged cluster with aggregation number, $s$, as a function of the Bjerrum length $l_B$ for the diblock polyampholyte with $N = 256$ and $f = 1/16$. Since the probability for finding multiplets with odd number of charges is very low (see also refs 56−58), the values of $P_s$ are only shown for the isolated charged monomers $s = 1$ and the multiplets with even number of charges $s = 2$, 4, 6, etc. As shown in Figure 12, the probability $P_1$ for a charged monomer to be unbound decreases monotonically with increasing Bjerrum length due to the charge pairing which is reflected by the increase of the probability $P_2$ for charged monomers to be in

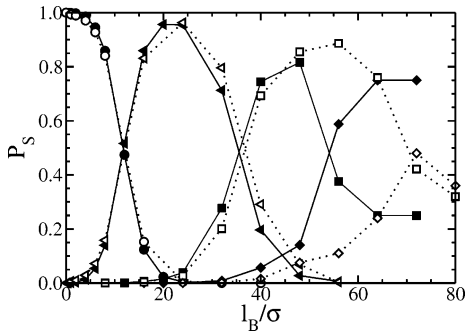


**Figure 12.** Probability for a charged monomer to be a part of a multiplet (cluster of charges) with aggregation number $s$ as a function of Bjerrum length $l_B$. Different symbols correspond to multiplets of different aggregation numbers: $s = 1$ (circles), $s = 2$ (triangles), $s = 4$ (squares), $s = 6$ (diamonds). The solid symbols are simulation results for a single diblock polyampholyte of $N = 256$ monomers and charge fraction $f = 1/16$. The open symbols are simulation results obtained in solutions of polymer chains each containing $N = 17$ monomers with only the middle monomer being charged. The number density of the charged monomers in the solution of single charged chains is $c_{sl} = 4.77 \times 10^{-3}\sigma^{-3}$. The solid (diblock polyampholytes) and dotted (solutions of single-charged chains) lines are guides to the eye.

dipoles. The $P_1(l_B)$ and $P_2(l_B)$ curves intersect at $l_B \approx 11.8\sigma$. At higher Bjerrum lengths, the value of $P_2$ is higher than $P_1$ and reaches its peak value ($P_2 \approx 0.96$) at $l_B \approx 20\sigma$, indicating that almost all charged monomers are paired in dipoles consistent with $\xi_{+-}^{1st} \approx \sigma$ in Figure 10. A further increase of the electrostatic interaction strength leads to the decrease of $P_2$ and the increase of the probability $P_4$ for a charged monomer to be a part of quadrupole. The intersection of the $P_2(l_B)$ and $P_4(l_B)$ curves at $l_B \approx 36\sigma$ indicates the transformation of multiplets from dipoles to quadrupoles. Similarly, quadrupoles transform to higher order multiplets (hexapoles, octupoles) at even larger values of $l_B$. The cascade of the multiplet formation transitions can be quantitatively determined from the intersections of the $P_s(l_B)$ curves, as shown above for the single charge to dipole transition ($l_B \approx 11.8\sigma$) and the dipole to quadrupole transition ($l_B \approx 36\sigma$). However, the determination of the transitions between higher order multiplets is somewhat ambiguous. The main problem is that the multiplets with larger number of charged monomers ($s \geq 6$) are formed at very high values of Bjerrum length where the system is almost frozen due to strong electrostatic interactions. We are developing more sophisticated simulation methods in order to obtain well-equilibrated polymer conformations for large Bjerrum lengths (e.g., $l_B \geq 40\sigma$) and will present our results in a future publication.

Each multiplet formed in diblock polyampholyte systems is surrounded by a corona formed by neutral chain sections linking the charged monomers. Such structures have similarities with the micelles formed in block copolymer solutions in selective solvents.[59−61] A multiplet with aggregation number $s$ formed in diblock polyampholyte systems is connected to $2s$ neutral chain sections (called arms) in the corona with $N_{arm} = 1/(2f)$ uncharged monomers in each arm. This differs from the multiplets formed in ionomer systems where the corona surrounding a multiplet with $s$ charges consists of only $s$ chain sections because half of the charges are counterions.[62−67] Multiplets with corona of $2s$ arms are also expected in solutions of random and multiblock polyampholytes and in complexes formed by mixtures of oppositely charged polyelectrolytes.[68]

**c. Solution of Charges with Two Neutral Tails.** To demonstrate the generality of the multiplet formation cascade, we have performed an independent set of simulations of solutions of short polymer chains, each containing $f^{-1} + 1$

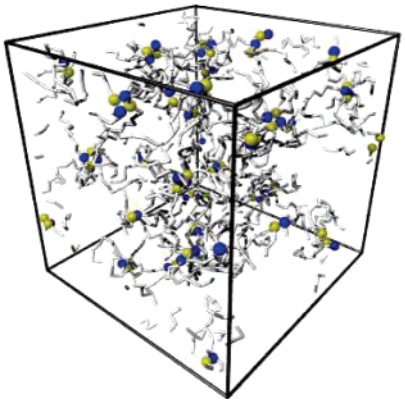

**Figure 13.** Snapshot of the solution of 17-mers with a single charge in the middle of each chain at Bjerrum length $l_B = 40\sigma$ in a good solvent. The number density of the charged monomers is $c_{sl} = 4.77 \times 10^{-3}\sigma^{-3}$, corresponding to the number density of charges inside the globule formed by a diblock polyampholyte chain with charge fraction $f = 1/16$ at the upper boundary of the weak association regime.

monomers with a single charge in the middle of the chain. Thus, each polymer chain consists of a single charged monomer connected to two uncharged tails (arms) with degree of polymerization $1/(2f)$ each. This corresponds to cutting a diblock polyampholyte chain with $N$ monomers and charge fraction $f$ into $fN$ segments by breaking the middle bond of each neutral spacer linking two sequential charged monomers. In our simulations there are 100 such short chains, half of them carrying a positive charge and half of them carrying a negative charge. The periodic boundary conditions are applied in all three directions of the simulation box. The number density of the chains, or equivalently the number density of the charged monomers, in the solution is chosen to be the overlap concentration of the short polymer chains. It corresponds to the charge density inside a globular diblock polyampholyte of charge fraction $f$ at the upper boundary of the weak association regime. Figure 13 presents a snapshot of the solution of polymers with $N = 17$ monomers and the number density of chains $c_{sl} = 4.77 \times 10^{-3}\sigma^{-3}$ in a good solvent at Bjerrum length $l_B = 40\sigma$.

The simulation results for the probability, $P_s$, of a charged monomer to be a part of a cluster with aggregation number, $s$, for the solution of short polymers with $N = 17$ monomers in a good solvent are presented by open symbols in Figure 12. The definition of clusters is the same as for diblock polyampholytes with the same cutoff distance $r_{cut} = 1.5\sigma$. The resulting curves for the Bjerrum length dependence of $P_s$ (dotted lines) almost coincide with those of the diblock polyampholyte with charge fraction $f = 1/16$ for cluster sizes $s \leq 4$ (solid lines) and correspondingly in the region of Bjerrum length $l_B \leq 50\sigma$. Since the total number of charges in the short chain solution (100) is several times larger than that in the single diblock polyampholyte ($fN = 16$), the agreement of the results for the distribution of cluster sizes in the two cases demonstrates that there is no evident finite size effect for Bjerrum length $l_B \leq 50\sigma$. This is also confirmed by the calculation of the average multiplet size $\langle s \rangle$, which is defined as

$$\langle s \rangle = \langle \sum_s sN_s / \sum_s N_s \rangle \tag{25}$$

where $N_s$ is the number of clusters containing $s$ charged monomers. The simulation results for $\langle s \rangle$ are plotted in Figure 14 as a function of Bjerrum length $l_B$ for the diblock polyampholytes with $N = 256$ monomers and different charge fractions $f$ (1/4, 1/8, and 1/16) and for the corresponding

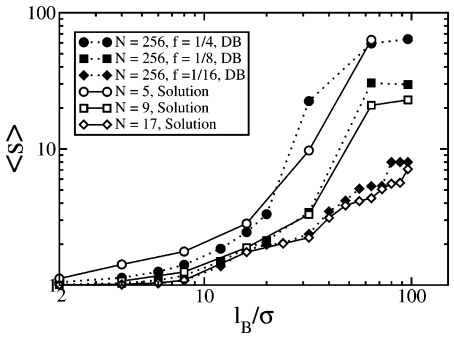


**Figure 14.** Average aggregation number $\langle s \rangle$ of the multiplets formed by charged monomers as a function of the Bjerrum length $l_B$. The solid symbols are simulation results for the diblock polyampholytes (DB) with degree of polymerization $N = 256$ and different charge fractions $f$ [$f = 1/4$ (circles), $f = 1/8$ (squares), and $f = 1/16$ (diamonds)] in a good solvent. The open symbols are simulation results for the solutions of polymers with a single charge on the middle monomer of each chain. The number densities of the charged monomers in the solutions are $c_{sl} = 8.11 \times 10^{-2}\sigma^{-3}$ ($N = 5$), $c_{sl} = 1.69 \times 10^{-2}\sigma^{-3}$ ($N = 9$), and $c_{sl} = 4.77 \times 10^{-3}\sigma^{-3}$ ($N = 17$), respectively.

solutions of short chains with different degrees of polymerization $N = f^{-1} + 1$. The results obtained for the two different classes of systems are in very good agreement. They show that the dependence of the average cluster size $\langle s \rangle$ on the Bjerrum length $l_B$ is stronger for the systems with larger charge fraction $f$. The results presented in Figures 12 and 14 suggest that the solution of short polymers with a single charge per chain could be used as a simplified model to discuss the cascade of multiplet formation transitions.

**d. The Boundary of the Ion Binding Regime.** The total free energy of a multiplet formed in a diblock polyampholyte or the corresponding solution of charges with two neutral tails consists of the Coulomb energy of the core formed by charged monomers, the conformational (for diblock polyampholyte) or translational (for the solution of short chains) entropy loss due to association of the charges, and the steric repulsion and elastic stretching energies of the neutral chain sections in the corona. Our numerical calculations have revealed that the Coulomb energy of the formed dipoles ($\propto -l_B k_B T/\sigma$ per charge) and the entropic penalty due to pairing of charges are the two dominant contributions of the free energy.

For a diblock polyampholyte with most oppositely charged monomers bound into dipoles, the conformational entropic penalty per charge has a logarithmic dependence on the concentration $c_{db}$ of charged monomers inside the globule $\sim k_B T \ln(c_{db}\sigma^3)$, analogous to that in a globule formed by an associative polymer with high fraction of associated stickers.[69,70] The charge concentration $c_{db}$ inside the globule upon charge pairing corresponds to the overlap of the neutral chain sections (spacers) between adjacent charges along the blocks, $c_{db} \sim (\xi_e^{min})^{-3} \sim f^{3\nu}/\sigma^3$ (see eq 22). Balancing the two dominant (Coulomb and entropic) terms of the free energy leads to the Bjerrum length $l_B^{bind}$ at the transition point from isolated charges to dipoles

$$l_B^{bind} \approx -\sigma \ln(c_{db}\sigma^3) \approx -\sigma \ln(f) \tag{26}$$

In simulations, $l_B^{bind}$ is taken to be the Bjerrum length at which the probability for a charged monomer to be in a dipole is equal to the probability for it to be isolated, as discussed above. The logarithmic dependence of $l_B^{bind}$ on the charge fraction $f$ is verified in Figure 4 by the simulation results of $l_B^{bind}$ (squares) for the diblock polyampholytes with $f \leq 1/4$ and the logarithmic fit to these data [line IV, $l_B^{bind} = \sigma(6.87 - 1.77 \ln f)$].

In the solutions of single charges with two neutral tails, the translational entropic loss per charge due to charge association is on the order of $k_BT \ln(c_{sl}\sigma^3)$, where $c_{sl}$ is the number density of the chains (and also of the charges). Recalling that the number density of charges $c_{sl}$ in these solutions is proportional to the overlap concentration of these short polymers with $f^{-1} + 1$ monomers in each chain, it gives $c_{sl} \approx f^{3\nu}/\sigma^3$, which is the same order as $c_{db}$ in the corresponding globule of diblock polyampholyte. Therefore, the lower boundary of the ion binding regime of the short polymer solution is also defined by eq 26. The values of $l_B^{bind}$ obtained from simulations of the corresponding short polymer solutions are almost the same as that of the diblock polyampholytes, as can be seen in Figure 12. It confirms that using the overlap concentration of the solutions of charges with two tails is essential to get the consistent results on multiplet formations for the two different systems.

Above the lower boundary (line IV in Figure 4), the ion binding regime can be further divided into separate domains corresponding to the regions where multiplets of different aggregation numbers dominate. In Figure 4 we present our preliminary simulation results for the dipole-to-quadrupole transition (triangles) and quadrupole-to-hexapole transition (diamonds) with dotted lines (V and VI), indicating our estimate for the boundary between these multiplet domains following eq 26 with different coefficients. In the region between lines IV and V, dipoles are the dominant multiplets, while quadrupoles dominate in the region between lines V and VI. Domains corresponding to multiplets with higher aggregation numbers can be observed at larger values of Bjerrum length with the progress of the cascade of multiplet formation transitions. A more accurate determination of the multiplet domains in the ion binding regime will be presented in a future publication.

The multiplet formation had also been noticed in the Monte Carlo simulations of telechelic polyampholytes (a neutral chain with a positive charge at one end and a negative charge at the other end).[30] The telechelic polyampholyte solution differs from the solution of charges with two neutral tails (and from diblock polyampholytes) because in telechelic polyampholytes there is only one neutral chain section connected to each charge. The results of the reciprocal critical temperatures (Bjerrum lengths at the critical point) obtained for the solution of telechelic polyampholytes are located between lines IV (dipole formation) and V (quadrupole formation) in Figure 4 and exhibit a similar logarithmic dependence on the charge fraction *f*. The two oppositely charged monomers from the same telechelic polyampholyte chain can associate with each other, forming an intramolecular dipole at any arbitrary low concentration. Therefore, the critical temperature related to phase separation reported in ref 30 corresponds to the formation of quadrupoles and multiplets of larger aggregation numbers. The critical Bjerrum length (reciprocal critical temperature) of the telechelic polyampholytes is lower than the Bjerrum length corresponding to the quadrupole formations (line V) in diblock polyampholytes and the solution of charges with two neutral tails due to the lower steric hindrance and entropic penalty of fewer neutral arms connected to each multiplet in the telechelic polyampholyte solution. The critical number density of charges for the telechelic polyampholyte solution is lower than the corresponding charge density in the solution of charge with two neutral tails. The charge densities in both cases follow a power law dependence on the charge fraction $c \sim f^{-3\nu}$ with $\nu \approx 0.588$ in a good solvent for neutral chain sections.

From a general point of view, the ionic binding regime studied in this work connects the regular polyelectrolyte (polyampholyte) behavior in polar solvents (weak electrostatic interaction strength) to ionomers in low-polarity media (strong electrostatic interaction strength).[46−48] The high values of $l_B$ can be experimentally obtained for charged polymers in air and in nonpolar or low-polarity solvents where the dielectric constant is very low (1 or 2). For example, the study of ionomers is mostly performed in polymer melts or in solvents of low dielectric constant (e.g., toluene with $\epsilon \approx 2$),[46−48,62,63,71] and multiplet formations have been analyzed in such low-polarity media.[62,63,71] Many AFM studies of the conformational properties of charged polymers are also performed at the air/solid interface where the polymers are in air (with $\epsilon \approx 1$).[72] The actual distance between the charged atoms at contact could be much smaller than the monomer size, which makes the electrostatic interactions even stronger, as discussed in the literature on ionomers.[62,63] Even for polyelectrolytes or polyampholytes dissolved in a polar solvent, the globular regions of these polymers (e.g., globules of pearl necklace conformations of hydrophobic polyelectrolytes or polyampholytes[4,5]) contain much less (or no) solvents. The charged monomers inside these regions are in the environment of low dielectric constant ($\epsilon \approx 2$) and therefore experience interactions with large local Bjerrum length in contrast to $\epsilon \approx 80$ and $l_B \approx 7$ Å outside the globules.

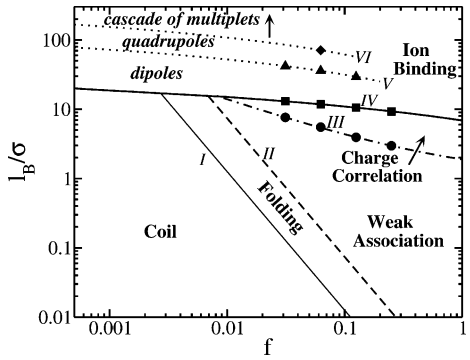


**Figure 15.** Diagram of conformational states of a symmetric diblock polyampholyte in the Bjerrum length, $l_B$, and charge fraction, *f*, plane in a good solvent. The lower boundary of the folding regime (thin solid line I) and the lower boundary of the weak association regime (dashed line II) are calculated for the degree of polymerization $N = 3000$. Other lines and symbols are the same as in Figure 4.

## 4. Discussion of the Diagram of States

The diagram of conformational states of a symmetric diblock polyampholyte in the Bjerrum length, $l_B$, and charge fraction, *f*, plane is presented in Figure 4 for a chain with $N = 256$ monomers in a good solvent condition. In this diagram the lower boundary of the folding regime (line I−eq 13) and the lower boundary of the weak association regime (line II−eq 15) depend on the degree of polymerization *N* of the diblock chain, but the upper boundary of the weak association regime (line III−eq 23), the lower boundary of the ion binding regime (line IV−eq 26), and the lines corresponding to the multiplet transitions in the ion binding regime (lines V, VI, etc.) are *N*-independent. Lines I and II in Figure 4 are presented for $N = 256$ corresponding to our MD simulations. We show another conformational diagram in Figure 15 where the lines I and II are calculated from eqs 13 and 15 for a much larger degree of polymerization $N = 3000$, while the other (*N*-independent) lines remain the same as in Figure 4. Comparing Figures 4 and 15, we see that lines I and II are shifted to lower charge fractions *f* with increasing number of monomers in the diblock chain. The width of the folding regime is not changed because the ratio between $l_B^{weak}$ and $l_B^{fold}$ is a numerical constant ($C_w/C_f \approx 6$

in a good solvent, see eqs 13 and 15). The width of the weak association regime, $l_B^{up}/l_B^{weak} \approx (fN)^{2-\nu}/C_w$ (see eqs 15 and 23), at a fixed value of charge fraction $f$ increases with increasing degree of polymerization $N$.

The upper boundary of the weak association regime (line III) has a power-law dependence on the charge fraction $f$ (eq 23), while the lower boundary of the ion binding regime (line IV) has a weaker logarithmic $f$ dependence (eq 26). The width of the charge correlation region between lines III and IV thus decreases with decreasing charge fraction. These two lines (III and IV) meet at $f \approx 0.0084$ (see Figures 4 and 15), and the charge correlation region does not exist at lower charge fractions.

In Figure 15 the ion binding regime cuts the weak association regime off, and the upper boundary of the weak association regime (for $0.007 < f < 0.0084$) is determined by eq 26 (line IV) instead of eq 23. The conformation of diblock polyampholytes changes directly from a classical globular state into ion binding (dipole formation) state with increasing strength of electrostatic interactions. The weak association regime completely disappears at lower charge fraction at which the lower boundary of the weak association regime (line II) intersects line IV corresponding to the onset of the ion binding regime, i.e., at $f^2 \ln f \approx -C_w N^{\nu-2}$ (see eqs 15 and 26). This intersection is at $f \approx 0.007$ for the diblock polyampholyte with $N = 3000$ monomers, as shown in Figure 15. For diblock polyampholytes with fewer monomers ($N \leq 2300$), the weak association regime ends at the intersection of lines II and III. As an example, for a diblock chain with $N = 256$ monomers this intersection occurs at charge fraction $f \approx 0.07$ (see Figure 4). At lower values of charge fraction ($f < 0.07$) this polyampholyte chain crosses over from the folding regime directly into the charge correlation region or ion binding regime upon increasing strength of electrostatic interactions (see Figure 4). The diblock polyampholyte with very low charge fraction can enter the ion binding regime with increasing $l_B$ even before it starts to fold. In this case the electrostatic attraction energy between the two oppositely charged blocks, $l_B k_B T (fN)^2/R_{g0}$, is smaller than $k_B T$ because the folding has not started yet, while the Bjerrum length $l_B \gg \sigma$, leading to pairing of oppositely charged monomers into dipoles.

A well-defined cascade of multiplet formations in the ion binding regime can only be observed for polymers with long neutral chain sections connected to charged monomers. The steric repulsion and conformational entropy of these neutral sections are large enough to stabilize the multiplets with different aggregation numbers. In diblock polyampholytes with high charge fractions ($f \geq 1/4$) and the corresponding solutions of charges with two short neutral tails, almost all charged monomers are found to aggregate into one cluster at a certain value of $l_B$ (e.g., $l_B \approx 60\sigma$ for $f = 1/4$ in Figure 14). These systems undergo a phase separation, which limits the cascade of multiplet formations at high charge fractions. The phase separation of short fully charged diblock polyampholytes ($N \leq 16$ and $f = 1$) has been observed in grand canonical Monte Carlo simulations.[30] In solutions of diblock polyampholytes with charge fraction $f = 1$ or 1/2, the monomers in the dense phase are packed, analogous to an ionic solid. For the diblock polyampholytes with $f = 1/4$, the steric hindrance of the uncharged chain sections prevent the uniform growth of the ionic cluster in all three directions. In this case the oppositely charged monomers prefer to arrange in an alternating way forming dipole chains or rings to lower the total free energy. The chains of dipoles with surrounding uncharged chain sections are similar to cylindrical micelles or molecular brushes,[60,73] while multiplets with small aggregation numbers and spherical uncharged corona are similar to spherical micelles. Therefore, the decrease in the number of monomers in the neutral chain sections leads to the increase of the average cluster size as well as to a sphere-to-cylinder transition of the cluster shape. This is similar to the sphere-to-cylinder transition of micelles formed in dilute solutions of neutral diblock copolymers in a selective solvent with the decrease of the degree of polymerization of the soluble blocks.[59,60] The formation of the chain of dipoles leads to the nonmonotonic behavior of the chain size $R_g$ in the ion binding regime of the diblock polyampholytes with high charge fraction $f$, as shown in Figure 1.

## 5. Conclusions

The conformational properties of an isolated diblock polyampholyte have been studied by extensive molecular dynamics simulations. The electrostatically driven coil−globule transition of a symmetric diblock polyampholyte is found to consist of three regimes identified with increasing interaction strength. In the first regime electrostatic attraction causes the chain to fold through an overlap of the two blocks, while each block is slightly stretched by the repulsion between charged monomers of the same sign. The folding process of the diblock chain can be well described by a simple model of two oppositely charged objects with either uniform or Gaussian monomer distributions jointed by an entropic spring. The second regime is the classical globule with the fluctuation-induced attraction between the oppositely charged chain sections. This attraction is stabilized by the two-body excluded-volume repulsions in a good solvent or three-body repulsion in a Θ-solvent. Since the electrostatic attraction energy per charged monomer is less than the thermal energy, this regime is called "weak association" or "scrambled egg" regime. The structure of the "scrambled egg" globule can be represented as a dense packing of the electrostatic blobs with oppositely charged blobs preferentially surrounding each other. We confirm the scaling theory prediction for the size of these blobs (eq 10) by monitoring the average distance between nearest oppositely charged monomers $\xi_{\pm}^{1st} \approx \xi_e$ (see Figure 8). Scaling theory predicts the universal dependence of the chain size in the weak association regime on the interaction parameter ($N^{2-\nu} l_B f^2/\sigma$) (see eq 18). This scaling is confirmed by our simulation results in both good and Θ-solvent conditions, as demonstrated in Figure 3. If the average electrostatic energy per charge is higher than the thermal energy, the oppositely charged monomers are strongly correlated and tend to bind with each other to form charge pairs (dipoles). The diblock chain enters the third (ion binding) regime when the probability for a charged monomer to be bound in a dipole is higher than that for it to stay unbound. We predict a cascade of multiplet formations with increasing strength of the electrostatic interactions, identified by charge pairing (dipole formation, line IV in Figures 4 and 15), dipole pairing (quadrupole formation, line V in Figures 4 and 15), and subsequent formations of larger multiplets (hexapoles, octupoles, etc.). The cascade of multiplet formation transitions has also been observed in our simulations of the solutions of short polymers with a single charge in the middle of each chain. This suggests that this cascade of multiplet formations is a general physical phenomenon that could be expected in many different charged polymer systems, such as mixtures of oppositely charged polyelectrolytes, solutions of either random or block polyampholytes, etc. The diagram of conformational states of diblock polyampholytes is constructed on the basis of results of simulations and scaling calculations.

**Acknowledgment.** We acknowledge Dr. S. Panyukov for very helpful discussions. The authors are grateful to the National Science Foundation for the financial support under grants CHE-9876674, CHE-0616925 and CTS-0609087.

## Appendix. Models of the Folding Regime

As sketched in the inset of Figure 5a, the diblock polyampholyte can be modeled by two oppositely charged objects of identical size with their centers of mass linked by an entropic spring. Below we represent individual blocks by objects with two different (uniform or Gaussian) monomer distributions.

**I. Uniform Monomer Distribution Model.** In the uniform monomer distribution model, the two individual blocks are represented by two oppositely charged spheres of identical radii $R_{sp} = (5/3)^{1/2}R_{g0,blk}$, where $R_{g0,blk}$ is the radius of gyration of an uncharged chain block. The number density of monomers inside the spheres is $\rho_s \equiv \rho_+ = \rho_- = 3N/(8\pi R_{sp}^3)$.

Because of the symmetry of the model system, its square radius of gyration $R_g^2$ is equal to

$$R_g^{\,2} = R_{g0,blk}^{\,2} + r_{cm}^{\,2}/4 \tag{A1}$$

where $r_{cm}$ is the distance between the centers of the two spheres and $R_{g0,blk}$ is the radius of gyration of each sphere. The ratio of the sizes of an uncharged symmetric diblock chain and of each block is $R_{g0}/R_{g0,blk} = 2^{\nu}$. Substituting this relation into eq A1, we conclude that the root-mean-square distance between centers of the blocks $r_{cm}$ in the case of the uncharged chain $r_{cm0} = 2(1 - 4^{-\nu})^{1/2}R_{g0}$ is smaller than the diameter of the spheres $2R_{sp} = 2^{1-\nu}(5/3)^{1/2}R_{g0}$ in both the good ($\nu = 0.588$) and Θ ($\nu = 0.5$) solvent conditions. Thus, the two spheres are, on average, partly overlapping with each other even in the uncharged case ($l_B = 0$).

The entropic potential $F^{ela}$ of the spring linking the two spherical blocks is assumed to have a simple harmonic form

$$F^{ela} = \frac{1}{2}Ak_BT\frac{r_{cm}^{\,2}}{r_{cm0}^{\,2}} \tag{A2}$$

where $A$ is the dimensionless spring constant. This potential is balanced by the short-range repulsive energy between the two overlapping blocks. The origin of the repulsive energy is either the two-body excluded volume interactions (good solvent) or three-body interactions (Θ-solvent) between monomers from different blocks in the overlapping volume. This short-range repulsive energy can be calculated by

$$F^{2-body} = Bk_BT\upsilon\int\rho^2(\mathbf{r})\,d\mathbf{r}^3 \tag{A3}$$

in good solvent condition and

$$F^{3-body} = Ck_BTw\int\rho^3(\mathbf{r})\,d\mathbf{r}^3 \tag{A4}$$

in Θ-solvent condition, respectively. Here $\upsilon \approx \sigma^3$ and $w \approx \sigma^6$ are the two- and three-body interaction parameters, and $B$ and $C$ are numerical coefficients. The total number density of monomers in space is $\rho(\mathbf{r}) = \rho_+(\mathbf{r}) + \rho_-(\mathbf{r})$, where $\rho_+(\mathbf{r})$ and $\rho_-(\mathbf{r})$ are constant within the volumes of the two oppositely charged spheres and zero outside them. The integrals in eqs A3 and A4 are taken over the overlapping region, and only the cross terms containing the multiplication of $\rho_+$ and $\rho_-$ need to be considered.

In the case of uniform monomer distribution, the two- and three-body interaction energies between the two spheres are

$$F^{2-body} = 2Bk_BT\upsilon\rho_s^{\,2}V_{overlap} \tag{A5}$$

$$F^{3-body} = 6Ck_BTw\rho_s^{\,3}V_{overlap} \tag{A6}$$

where

$$V_{overlap} = \frac{\pi}{12}(16R_{sp}^{\,3} - 12R_{sp}^{\,2}r_{cm} + r_{cm}^{\,3}) \tag{A7}$$

is the overlapping volume of the two spheres, and the monomer number density in each sphere is $\rho_s \equiv \rho_+ = \rho_-$.

The free energy of the model system in the uncharged case is

$$F_0 = F^{ela} + F^{2(3)-body} \tag{A8}$$

The probability for the two spheres at a center-to-center distance $r_{cm}$ is proportional to the Boltzmann factor $\exp(-F_0/k_BT)$. The unperturbed mean-square radius of gyration of the model system (and of the diblock chain), $R_{g0}^2$, can thus be calculated as

$$R_{g0}^{\,2} = \frac{\int_0^\infty R_g^{\,2}\exp(-F_0/k_BT)r_{cm}^{\,2}\,dr_{cm}}{\int_0^\infty \exp(-F_0/k_BT)r_{cm}^{\,2}\,dr_{cm}} \tag{A9}$$

where $R_g^2$ in the integral of the numerator is defined by eq A1. In our simulations, the dependence of the unperturbed radius of gyration $R_{g0}$ on the degree of polymerization $N$ is found to be $R_{g0} \approx 0.46N^{\nu}\sigma$ in both the good and Θ-solvent conditions with the difference between the two cases in the third significant digit of the numerical prefactor. Using this $N$ dependence of $R_{g0}$, eq A9 determines the relation of the coefficients $B$ and $C$ in eqs A5 and A6 with the dimensionless spring constant $A$ in the elastic potential.

The electrostatic energy of the model system consists of two parts: the self-energy of each individual block and the attraction energy between the two oppositely charged blocks. The electrostatic self-energy of a uniformly charged sphere with magnitude of charge $Q \equiv Q^*e = Nfe/2$ is $3Q^{*2}l_Bk_BT/5R_{sp}$. The electrostatic attraction energy $F^{el}$ between two uniformly and oppositely charged spheres is given by[74]

$$F^{el}(r_{cm}) = -Q^{*2}l_Bk_BT \times \begin{cases} \dfrac{1}{R_{sp}}\left(\dfrac{6}{5} - \dfrac{r_{cm}^{\,2}}{2R_{sp}^{\,2}} + \dfrac{3r_{cm}^{\,3}}{16R_{sp}^{\,3}} - \dfrac{r_{cm}^{\,5}}{160R_{sp}^{\,5}}\right) & r_{cm} \le 2R_{sp} \\ \dfrac{1}{r_{cm}} & r_{cm} \ge 2R_{sp} \end{cases} \tag{A10}$$

The function $F^{el}(r_{cm})$ (eq A10) is plotted by the solid line in Figure 16. It can be seen that the strength of the attraction energy $F^{el}$ increases with the decrease of $r_{cm}$, while the self-energy of each block is constant. As a result, the total electrostatic energy of the model system decreases with the decrease of the separation between the two blocks and approaches zero when the two blocks completely overlap with each other ($r_{cm} = 0$). Since the self-energy of each block is constant, we only keep the attraction part of the electrostatic energy, $F^{el}$, in the total free energy of the model system for the following calculations.

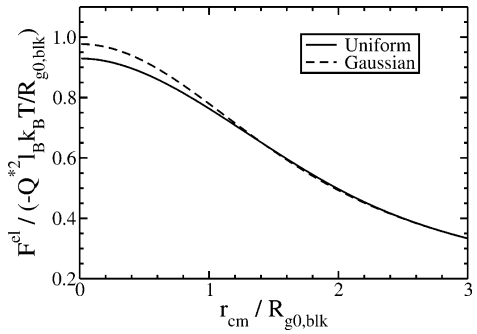


**Figure 16.** Electrostatic potential $F^{el}$ between two oppositely charged objects with uniform charge distribution (solid line) obtained from eq A10 and with Gaussian charge distribution (dashed line) obtained from eq A21.

The total free energy $F$ of the model system with electrostatic interactions is

$$F = F^{ela} + F^{2(3)-body} + F^{el} \tag{A11}$$

The mean-square radius of gyration, $\langle R_g^2 \rangle$, of the model system at different values of $l_B$ can be calculated by

$$\langle R_g^2 \rangle = \frac{\int_0^\infty R_g^2 \exp(-F/k_BT) r_{cm}^2 \, dr_{cm}}{\int_0^\infty \exp(-F/k_BT) r_{cm}^2 \, dr_{cm}} \tag{A12}$$

The numerical results of the rescaled radius of gyration, $\langle R_g^2 \rangle^{1/2}/R_{g0}$, with increasing electrostatic attraction are plotted as dashed lines in Figure 5, together with the simulation results (symbols) for both the good (Figure 5a) and Θ (Figure 5b) solvent conditions. In these calculations the value of the spring constant $A$ is taken to be $A = 4.7$ in good solvent condition and $A = 4$ in Θ-solvent condition. Accordingly, the values of the two- and three-body interaction parameters (eqs A5 and A6) are obtained from eq A9 as $B = 2.9/(R_{g0}/\sigma)^{0.4}$ and $C = 0.4$. We have also calculated the mean-square values of $r_{cm}$ and $R_g$ using the free energy minimization ($dF/dr_{cm} = 0$). Similar results for $\langle R_g^2 \rangle^{1/2}/R_{g0}$ have been achieved using a slightly different set of parameters $A$, $B$, and $C$.

**II. Gaussian Monomer Distribution Model.** In the Gaussian monomer distribution model, the $N/2$ monomers of each block are assumed to have a Gaussian distribution around the centers of mass of the corresponding blocks (see eq 14)

$$\rho_G(r) = \frac{N/2}{(\pi\alpha^2)^{3/2}} \exp(-r^2/\alpha^2) \tag{A13}$$

where $\alpha/\sqrt{2}$ ($= R_{g0,blk}/\sqrt{3}$) is the standard deviation. The two- and three-body interaction energies between the two blocks are calculated by introducing $\rho(\mathbf{r}) = \rho_{G+}(\mathbf{r}) + \rho_{G-}(\mathbf{r})$ with

$$\rho_{G+}(r) = \frac{N/2}{(\pi\alpha^2)^{3/2}} \exp(-r^2/\alpha^2) \tag{A14}$$

$$\rho_{G-}(r) = \frac{N/2}{(\pi\alpha^2)^{3/2}} \exp[-(r^2 + r_{cm}^2 - 2\mathbf{r}\cdot\mathbf{r}_{cm})/\alpha^2] \tag{A15}$$

into eqs A3 and A4, respectively. The vector $\mathbf{r}$ is measured from the center of mass of one (e.g., positively charged) block, and $\mathbf{r}_{cm}$ is the vector between the centers of mass of the two blocks. The nonelectrostatic interaction energies between the two blocks can be shown to be Gaussian functions of the distance $r_{cm}$

$$F^{2-body} = Bk_BTv \frac{N^2}{4\sqrt{2}\pi^{3/2}\alpha^3} \exp(-r_{cm}^2/2\alpha^2) \tag{A16}$$

$$F^{3-body} = Ck_BTw \frac{N^3}{4\sqrt{3}\pi^3\alpha^6} \exp(-2r_{cm}^2/3\alpha^2) \tag{A17}$$

The electrostatic attraction energy $F^{el}$ between two Gaussian charge distributions, each carrying a total charge of the same value $Q \equiv Q^*e = Nfe/2$ but of the opposite sign, can be written as

$$F^{el}(r_{cm}) = -l_B f^2 k_B T \int_{-\infty}^{\infty} \rho_G(\mathbf{r}_+) \, d\mathbf{r}_+ \int_{-\infty}^{\infty} \rho_G(\mathbf{r}_-) \, d\mathbf{r}_- \frac{1}{|\mathbf{r}_+ - \mathbf{r}_- - \mathbf{r}_{cm}|} \tag{A18}$$

Equation A18 can be solved using the Fourier transformations of the functions

$$\rho_G(\mathbf{r}_{+(-)}) = \frac{N}{2} \int_{-\infty}^{\infty} \exp(-\pi^2 q_{+(-)}^2 \alpha^2) \exp(-2\pi i \mathbf{q}_{+(-)}\cdot\mathbf{r}) \, d\mathbf{q}_{+(-)} \tag{A19}$$

$$\frac{1}{|\mathbf{r}_+ - \mathbf{r}_- - \mathbf{r}_{cm}|} = \int_{-\infty}^{\infty} \frac{1}{q^2\pi} \exp[2\pi i \mathbf{q}\cdot(\mathbf{r}_+ - \mathbf{r}_- - \mathbf{r}_{cm})] \, d\mathbf{q} \tag{A20}$$

where $\mathbf{q}_{+(-)}$ and $\mathbf{q}$ are the reciprocal vectors. The electrostatic interaction energy becomes

$$F^{el}(r_{cm}) = -Q^{*2} l_B k_B T \frac{2}{\pi r_{cm}} \int_0^\infty \exp\left(-t^2 \frac{\alpha^2}{2r_{cm}}\right) \frac{\sin(t)}{t} \, dt = -Q^{*2} l_B k_B T \frac{\mathrm{erf}(r_{cm}/\sqrt{2}\alpha)}{r_{cm}} \tag{A21}$$

where $\mathrm{erf}(x) = (2/\sqrt{\pi}) \int_0^x \exp(-t^2) \, dt$ is the error function. The $F^{el}(r_{cm})$ function (eq A21) is plotted in Figure 16 as the dashed line. A similar calculation of the electrostatic energy between two Gaussian charge distributions is presented in ref 75. The electrostatic self-energy of each Gaussian charge distribution is $Q^{*2} l_B k_B T/\sqrt{2\pi}\alpha$, which is constant and does not need to be included in the total free energy for the calculation of the average radius of gyration of the model system (eq A12).

The mean-square radius of gyration, $\langle R_g^2 \rangle$, of the model system with Gaussian monomer distribution is calculated in the same way as that for the uniform monomer distribution model. The numerical results of $\langle R_g^2 \rangle^{1/2}/R_{g0}$ are presented by the dashed−dotted lines in Figure 5a,b. Here the value of the spring constant $A$ is taken to be $A = 5.1$ for good solvent condition and $A = 4$ for the Θ-solvent condition. The values of the numerical coefficients in the two-body (eq A16) and three-body (eq A17) interaction energies of the Gaussian monomer distribution are found to be $B = 2.9/(R_{g0}/\sigma)^{0.4}$ in the good solvent condition and $C = 0.28$ in the Θ-solvent condition.

## References and Notes

(1) Hara, M., Ed. *Polyelectrolytes*; Marcel Dekker: New York, 1993.
(2) Schmitz, K. S. *Macroions in Solution and Colloidal Suspension*; VCH: New York, 1993.
(3) Candau, F.; Joanny, J.-F. In *Polymeric Materials Encyclopedia*; Salamone, J. C., Ed.; CRC Press: Boca Raton, FL, 1996; pp 5476−5488.
(4) Dobrynin, A. V.; Colby, R. H.; Rubinstein, M. *J. Polym. Sci., Part B: Polym. Phys.* **2004**, *42*, 3513−3538.

(5) Dobrynin, A. V.; Rubinstein, M. *Prog. Polym. Sci.* **2005**, *30*, 1049−1118.
(6) Borue, V. Y.; Erukhimovich, I. Y. *Macromolecules* **1990**, *23*, 3625−3632.
(7) Tsuchida, E. *J. Macromol. Sci., Pure Appl. Chem.* **1994**, *A31*, 1−15.
(8) Srivastava, D.; Muthukumar, M. *Macromolecules* **1994**, *27*, 1461−1465.
(9) Kabanov, A. V.; Bronich, T. K.; Kabanov, V. A.; Yu, K.; Eisenberg, A. *Macromolecules* **1996**, *29*, 6797−6802.
(10) Pogodina, N. V.; Tsvetkov, N. V. *Macromolecules* **1997**, *30*, 4897−4904.
(11) Everaers, R.; Johner, A.; Joanny, J.-F. *Macromolecules* **1997**, *30*, 8478−8498.
(12) Tanaka, M.; Grosberg, A. Y.; Tanaka, T. *J. Chem. Phys.* **1999**, *110*, 8176−8188.
(13) Castelnovo, M.; Joanny, J. F. *Eur. Phys. J. E* **2001**, *6*, 377−386.
(14) Winkler, R. W.; Steinhauser, M. O.; Reineker, P. *Phys. Rev. E* **2002**, *66*, 021802.
(15) Hayashi, Y.; Ullner, M.; Linse, P. *J. Phys. Chem. B* **2003**, *107*, 8198−8207.
(16) Zhang, R.; Shklovskii, B. I. *Physica A* **2005**, *352*, 216−238.
(17) Kantor, Y.; Kardar, M. *Europhys. Lett.* **1994**, *27*, 643−648.
(18) Kantor, Y.; Kardar, M. *Phys. Rev. E* **1995**, *51*, 1299−1312.
(19) Yamakov, V.; Milchev, A.; Limbach, H. J.; Dunweg, B.; Everaers, R. *Phys. Rev. Lett.* **2000**, *85*, 4305−4308.
(20) Lee, N.; Thirumalai, D. *J. Chem. Phys.* **2000**, *113*, 5126−5129.
(21) Goloub, T.; de Keizer, A.; Stuart, M. A. C. *Macromolecules* **1999**, *32*, 8441−8446.
(22) Gohy, J.-F.; Creutz, S.; Garcia, M.; Mahltig, B.; Stamm, M.; Jerome, R. *Macromolecules* **2000**, *33*, 6378−6387.
(23) Mahltig, B.; Gohy, J.-F.; Jerome, R.; Stamm, M. *J. Polym. Sci., Part B: Polym. Phys.* **2001**, *39*, 709−718.
(24) Castelnovo, M.; Joanny, J. F. *Macromolecules* **2002**, *35*, 4531−4538.
(25) Shusharina, N. P.; Zhulina, E. B.; Dobrynin, A. V.; Rubinstein, M. *Macromolecules* **2005**, *38*, 8870−8881.
(26) Michaels, A. S. *Ind. Eng. Chem.* **1965**, *57*, 32−40.
(27) Philipp, B.; Dautzenberg, H.; K. J. Linow, J. K.; Dawydoff, W. *Prog. Polym. Sci.* **1989**, *14*, 91−172.
(28) Imbert, J. B.; Victor, J. M.; Tsunekawa, N.; Hiwatari, Y. *Phys. Lett. A* **1999**, *258*, 92−98.
(29) Baumketner, A.; Shimizu, H.; Isobe, M.; Hiwatari, Y. *J. Phys.: Condens. Matter* **2001**, *13*, 10279−10291.
(30) Cheong, D. W.; Panagiotopoulos, A. Z. *Mol. Phys.* **2005**, *103*, 3031−3044.
(31) Akinchina, A.; Shusharina, N. P.; Linse, P. *Langmuir* **2004**, *20*, 10351−10360.
(32) Victor, J. M.; Imbert, J. B. *Europhys. Lett.* **1993**, *24*, 189−195.
(33) Lee, N.; Obukhov, S. *Eur. Phys. J. B* **1998**, *1*, 371−376.
(34) Tanaka, M.; Grosberg, A. Y.; Tanaka, T. *Langmuir* **1999**, *15*, 4052−4055.
(35) Wittmer, J.; Johner, A.; Joanny, J.-F. *Europhys. Lett.* **1993**, *24*, 263−268.
(36) Kantor, Y.; Kardar, M. *Europhys. Lett.* **1991**, *14*, 421−426.
(37) Higgs, P. G.; Joanny, J.-F. *J. Chem. Phys.* **1991**, *94*, 1543−1554.
(38) Dobrynin, A. V.; Rubinstein, M. *J. Phys. II* **1995**, *5*, 677−695.
(39) Stevens, M. J.; Kremer, K. *J. Chem. Phys.* **1995**, *103*, 1669−1690.
(40) Micka, U.; Holm, C.; Kremer, K. *Langmuir* **1999**, *15*, 4033−4044.
(41) Kremer, K.; Grest, G. S. *J. Chem. Phys.* **1990**, *92*, 5057−5086.
(42) Hockney, R. W.; Eastwood, J. W. *Computer Simulation Using Particles*; Bristol IOP: Bristol, 1988.
(43) Deserno, M.; Holm, C. *J. Chem. Phys.* **1998**, *109*, 7678−7693.
(44) Deserno, M.; Holm, C. *J. Chem. Phys.* **1998**, *109*, 7694−7701.
(45) Allen, M. P.; Tildesley, D. J. *Computer Simulation of Liquids*; Oxford Science Publications Clarendon Press: Oxford, 1987.
(46) Lundberg, R. D.; Phillips, R. R. *J. Polym. Sci., Polym. Phys. Ed.* **1982**, *20*, 1143−1154.
(47) Bakeev, K. N.; Shu, Y. M.; Zezin, A. B.; Kabanov, V. A.; Lezov, A. V.; Melnikov, A. B.; Kolomiets, I. P.; Rjumtsev, E. I.; MacKnight, W. J. *Macromolecules* **1996**, *29*, 1320−1325.
(48) Nomula, S.; Cooper, S. L. *Macromolecules* **2001**, *34*, 925−930.
(49) de Gennes, P. G.; Pincus, P.; Velasco, R. M.; Brochard, F. *J. Phys. (Paris)* **1976**, *37*, 1461−1473.
(50) Rubinstein, M.; Colby, R. H.; Dobrynin, A. V. *Phys. Rev. Lett.* **1994**, *73*.
(51) The use of term "folding" does not imply that this conformational regime of diblock polymapholytes is related to "protein folding".
(52) The uncertainty in these values is from fitting different central fractions of the data points in the folding regime, ranging from 25% to 75%.
(53) Castelnovo, M.; Joanny, J. F. *Langmuir* **2000**, *16*, 7524−7532.
(54) Landau, L. D.; Lifshitz, E. M. *Statistical Physics*, 3rd ed.; Pergamon Press: Elmsford, NY, 1980; Part 1.
(55) Hayashi, Y.; Ullner, M.; Linse, P. *J. Chem. Phys.* **2002**, *116*, 6836−6845.
(56) Gillan, M. J. *Mol. Phys.* **1983**, *49*, 421−442.
(57) Caillol, J. M.; Weis, J. J. *J. Chem. Phys.* **1995**, *102*, 7610−7621.
(58) Yan, Q.; de Pablo, J. J. *J. Chem. Phys.* **2001**, *114*, 1727−1731.
(59) Halperin, A.; Tirrell, M.; Lodge, T. P. *Adv. Polym. Sci.* **1992**, *100*, 31−71.
(60) Zhulina, E. B.; Adam, M.; LaRue, I.; Sheiko, S. S.; Rubinstein, M. *Macromolecules* **2005**, *38*, 5330−5351.
(61) Kramarenko, E. Y.; Khokhlov, A. R.; Reineker, P. *J. Chem. Phys.* **2003**, *119*, 4945−4952.
(62) Eisenberg, A. *Macromolecules* **1970**, *3*, 147−154.
(63) Dreyfus, B. *Macromolecules* **1985**, *18*, 284−292.
(64) Williams, C. E.; Russell, T. P.; Jerome, R.; Horrion, J. *Macromolecules* **1986**, *19*, 2877−2884.
(65) Nyrkova, I. A.; Khokhlov, A. R.; Doi, M. *Macromolecules* **1993**, *26*, 3601−3610.
(66) Semenov, A. N.; Nyrkova, I. A.; Khokhlov, A. R. *Macromolecules* **1995**, *28*, 7491−7500.
(67) Semenov, A. N.; Nyrkova, I. A.; Khokhlov, A. R In *Ionomers: Characterization, Theory and Applications*; Schlick, S., Ed.; CRC Press: Boca Raton, FL, 1996; pp 251−279.
(68) Moldakarimov, S. B.; Kramarenko, E. Y.; Khokhlov, A. R.; Kudaibergenov, S. E. *Macromol. Theory Simul.* **2001**, *10*, 780−788.
(69) Lifshitz, I. M.; Grosberg, A. Y.; Khokhlov, A. R. *Rev. Mod. Phys.* **1978**, *50*, 683−713.
(70) Semenov, A. N.; Rubinstein, M. *Macromolecules* **1998**, *31*, 1373−1385.
(71) Schlick, S., Ed.; *Ionomers: Characterization, Theory, and Applications*; CRC Press: Boca Raton, FL, 1996.
(72) Minko, S.; Roiter, Y. *Curr. Opin. Colloid Interface Sci.* **2005**, *10*, 9−15.
(73) Dziezok, P.; Sheiko, S. S.; Fischer, K.; Schmidt, M.; Moller, M. *Angew. Chem., Int. Ed. Engl.* **1997**, *36*, 2812−2815.
(74) Jain, A. K.; Gupta, M. C.; Shastry, C. S. *Phys. Rev. C* **1975**, *12*, 801−805.
(75) Koniezny, M.; Likos, C. N.; Lowen, H. *J. Chem. Phys.* **2004**, *121*, 4913−4924.

MA0607517